NASA Technical Memorandum 113169 ARL–TR–1565

Determination of Creep Behavior of Thermal Barrier Coatings Under Laser Imposed Temperature and Stress Gradients

Dongming Zhu and Robert A. Miller
Lewis Research Center, Cleveland, Ohio

November 1997

The NASA STI Program Office ... in Profile

Since its founding, NASA has been dedicated to the advancement of aeronautics and space science. The NASA Scientific and Technical Information (STI) Program Office plays a key part in helping NASA maintain this important role.

The NASA STI Program Office is operated by Langley Research Center, the lead center for NASA's scientific and technical information. The NASA STI Program Office provides access to the NASA STI Database, the largest collection of aeronautical and space science STI in the world. The Program Office is also NASA's institutional mechanism for disseminating the results of its research and development activities. These results are published by NASA in the NASA STI Report Series, which includes the following report types:

- TECHNICAL PUBLICATION. Reports of completed research or a major significant phase of research that present the results of NASA programs and include extensive data or theoretical analysis. Includes compilations of significant scientific and technical data and information deemed to be of continuing reference value. NASA counter-part of peer reviewed formal professional papers, but having less stringent limitations on manuscript length and extent of graphic presentations.

- TECHNICAL MEMORANDUM. Scientific and technical findings that are preliminary or of specialized interest, e.g., quick release reports, working papers, and bibliographies that contain minimal annotation. Does not contain extensive analysis.

- CONTRACTOR REPORT. Scientific and technical findings by NASA-sponsored contractors and grantees.

- CONFERENCE PUBLICATION. Collected papers from scientific and technical conferences, symposia, seminars, or other meetings sponsored or co-sponsored by NASA.

- SPECIAL PUBLICATION. Scientific, technical, or historical information from NASA programs, projects, and missions, often concerned with subjects having substantial public interest.

- TECHNICAL TRANSLATION. English-language translations of foreign scientific and technical material pertinent to NASA's mission.

Specialized services that help round out the STI Program Office's diverse offerings include creating custom thesauri, building customized databases, organizing and publishing research results ... even providing videos.

For more information about the NASA STI Program Office, you can:

- Access the NASA STI Program Home Page at http://www.sti.nasa.gov/STI-homepage.html

- E-mail your question via the Internet to help@sti.nasa.gov

- Fax your question to the NASA Access Help Desk at (301) 621-0134

- Phone the NASA Access Help Desk at (301) 621-0390

- Write to:
  NASA Access Help Desk
  NASA Center for AeroSpace Information
  800 Elkridge Landing Road
  Linthicum Heights, MD 21090-2934

NASA Technical Memorandum 113169

ARL-TR-1565

Determination of Creep Behavior of Thermal Barrier Coatings Under Laser Imposed Temperature and Stress Gradients

Dongming Zhu and Robert A. Miller
Lewis Research Center, Cleveland, Ohio

National Aeronautics and
Space Administration

Lewis Research Center

November 1997

Available from

NASA Center for Aerospace Information
800 Elkridge Landing Road
Linthicum Heights, MD 21090-2934
Price Code: A03

National Technical Information Service
5287 Port Royal Road
Springfield, VA 22100
Price Code: A03

DETERMINATION OF CREEP BEHAVIOR OF THERMAL BARRIER COATINGS UNDER LASER IMPOSED TEMPERATURE AND STRESS GRADIENTS

Dongming Zhu † and Robert A. Miller
National Aeronautics and Space Administration
Lewis Research Center, Cleveland, OH 44135

ABSTRACT

In the present study, a laser sintering/creep technique has been established to quantitatively determine the creep behavior of thermal barrier coatings under steady state high heat flux/high thermal gradient conditions. An approach is proposed to separate the strong influence of stress relaxation, based on the deduced strain rate changes with respect to time and temperature during testing. For a plasma sprayed zirconia-8wt.% yttria ceramic coating, a large primary creep strain and a low creep activation energy were observed. The significant primary creep stage and low apparent creep activation energy for the coating are attributed to stress induced mechanical sliding, and temperature and stress enhanced cation diffusion through the splat and grain boundaries. Possible creep mechanisms for the ceramic coating are also discussed. The elastic modulus evolution, the stress response and the total accumulated creep strain variation across the ceramic coating under laser imposed temperature and stress conditions are simulated using a finite difference approach. The modeled creep response is consistent with experimental observations.

INTRODUCTION

Plasma-sprayed ceramic thermal barrier coatings have been developed for advanced gas turbine and diesel engine components to improve engine durability and efficiency [1-5] . However, the reliability of the coating systems remains a crucial issue under high temperature thermal cycling conditions. The coating failure mechanisms, which strongly depend on coating systems and operating conditions, are complex. Coating delamination and spallation might occur due to thermal expansion mismatch and bond coat oxidation in the coating system. Ceramic sintering and creep at high temperatures, resulting in coating shrinkage and through-thickness cracking during cooling [6-8] , will further accelerate the coating failure process [9]. The ceramic coating creep properties and creep related coating durability issues have long been recognized [10-14] . In addition,

† National Research Council — NASA Research Associate at Lewis Research Center.

Keywords: Thermal Barrier Coating, Laser Sintering and Creep, Elastic Modulus Evolution, Stress Relaxation

changes in thermomechanical and thermophysical properties as a result of coating sintering, such as the increase in coating elastic modulus and thermal conductivity, are also detrimental to coating fatigue resistance and performance. Therefore, determination of the sintering and creep behavior of plasma-sprayed thermal barrier coatings is of great importance. Also, future development of advanced sintering and creep resistant ceramic coatings will greatly benefit from reliable test methods that can efficiently and accurately evaluate coating sintering and creep properties under simulated engine temperature and stress conditions. In this paper, a laser sintering and creep technique having a high strain measurement sensitivity is developed and applied to thermal barrier coating configurations. Because of the laser imposed temperature and stress gradients across the coating system, the sintering and creep behavior of the ceramic coating is assessed from a set of integrated temperature and stress gradient experiments that are conducted for various test times. This approach is used to construct a creep constitutive equation for a plasma-sprayed ZrO_2-8wt.%Y_2O_3 ceramic coating. The elastic modulus evolution, stress response and the total accumulated creep strain variation across the ceramic coating under laser imposed temperature and stress conditions are simulated using a finite difference approach. The sintering and creep mechanisms based on experimental results are also discussed.

PRINCIPLES OF A LASER SINTERING/CREEP APPROACH FOR THERMAL BARRIER COATING SYSTEMS

Ceramic Coating Creep Response under Laser Heating Conditions

For a thermal barrier coating system consisting of a top ceramic coating, an intermediate metallic bond coat and a metal substrate, a steep temperature gradient and thus a stress gradient will be established across the ceramic coating under steady state laser heating conditions. The temperature and stress gradients imposed by the laser beam depend on laser heat flux, ceramic surface temperature, as well as material properties and configurations of the coating system [8]. In the absence of bending or coating delamination, a creep strain gradient due to the temperature and stress gradients can result in wedge-shape crack opening displacements across the ceramic coating after cooling. This is schematically shown in Figure 1. Since plasma sprayed thermal barrier coatings possess a long primary creep stage [15], the creep strain rate in the ceramic coating is not only a function of temperature and stress state, but also of time. In general, the primary creep strain rate can be expressed as [16]

$$\dot{\varepsilon}_p = A \cdot \exp\left(-\frac{Q}{RT}\right) \cdot \sigma^n \cdot t^{-s} \tag{1}$$

where $\dot{\varepsilon}_p$ is the creep strain rate, A, n and s are constants, Q is the creep activation energy, T is temperature, t is time, R is the gas constant, σ is the applied stress in the coating. During the laser creep testing, the stress term in Equation (1) needs to be replaced by the compressive thermoelastic stress induced in the coating. The time, temperature and stress dependent deformation can result in coating shrinkage in the loading direction, and thus stress relaxation, at temperature under the compressive stresses. The strain rate $\dot{\varepsilon}_p$ under the laser induced temperature and in-plane biaxial thermal stress conditions can be expressed using a modified version of Equation (1), as

$$\dot{\varepsilon}_p^i = A \cdot \exp\left(-\frac{Q}{RT}\right) \cdot \left\{\sigma_0 - \varepsilon_p{}^{i-1} \frac{E_c}{1-\nu_c}\right\}^n \cdot t_i^{-s} \tag{2}$$

where $\dot{\varepsilon}_p^i$ and $\varepsilon_p{}^{i-1}$ are the creep strain rate at time t_i and the total accumulated strain at the previous time step t_{i-1}, respectively, σ_0 is the initial thermal stress in the coating, E_c and ν_c are the elastic modulus and Poisson's ratio of the ceramic coating. The creep behavior of a thermal barrier coating, described by the constant A, the activation energy Q, and the stress and time exponents n and s, need to be determined experimentally. For the case of constant modulus, the total creep strain at any given time can be expressed as (Appendix A)

$$\varepsilon_p = \left\{\sigma_0 - \left[\sigma_0^{1-n} - A \cdot \frac{E_c(1-n)}{(1-\nu_c)(1-s)} \cdot \exp\left(-\frac{Q}{RT}\right) \cdot t^{1-s}\right]^{\frac{1}{1-n}}\right\} \cdot \frac{1-\nu_c}{E_c} \tag{3}$$

Equation (3) shows that the accumulated creep strain in the ceramic coating depends on time, temperature and stress, as well as the material properties. As shown in Figure 2, the kinetics of the coating shrinkage predicted from Equation (3), which in the present experiments will be observed as the kinetics of crack opening displacement and crack penetration depth after cooling, are very sensitive to the materials intrinsic creep characteristics [8, 17]. Figure 3 illustrates the calculated crack opening displacements at the ceramic surface and crack penetration depth as a function of laser heating time, for various creep parameters. It can be seen that the crack opening rate and crack penetration depth increase with increasing stress exponent, decreasing time exponent, and decreasing creep activation energy. Thus, the ceramic coating behavior under laser heating conditions in a thermal barrier coating system, provides a basis for determination of creep behavior using the laser sintering and creep technique described in this paper.

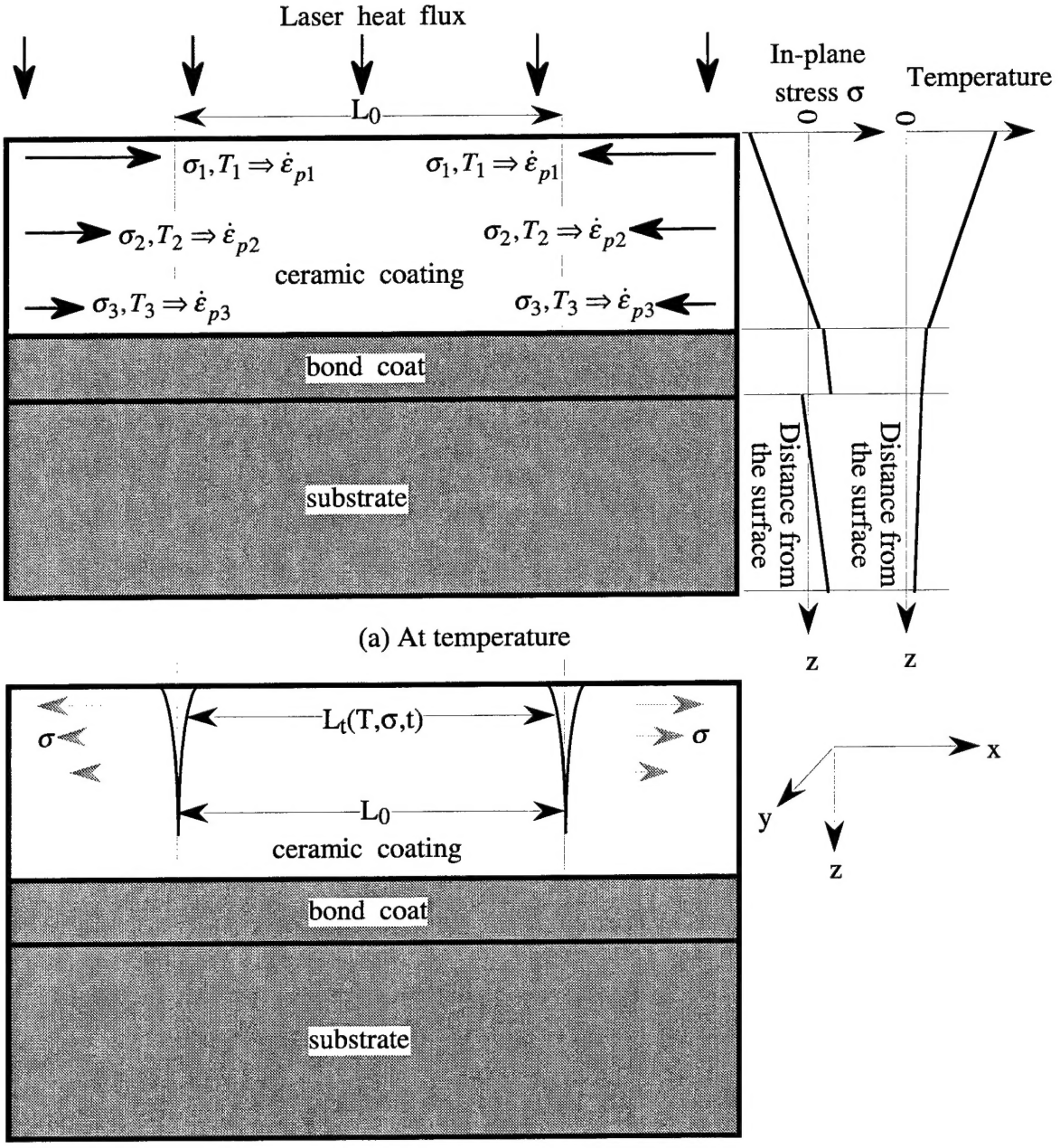

Fig. 1 Schematic diagram showing the principles of the laser sintering and creep test for thermal barrier coatings. (a) At temperature, different in-plane creep strain rates at various coating depths result from the in-plane stress and temperature gradients imposed by the laser heat flux; (b) After cooling, wedge-shape cracks develop as a result of the creep induced tensile stresses during cooling. Under a given laser test condition, the relative length change of the coating segment from L_0 at the initial time to $L_t(T,\sigma,t)$ at time t, can be used to determine the creep strains and thus strain rates in the ceramic coating at temperature as a function of stress, temperature and time.

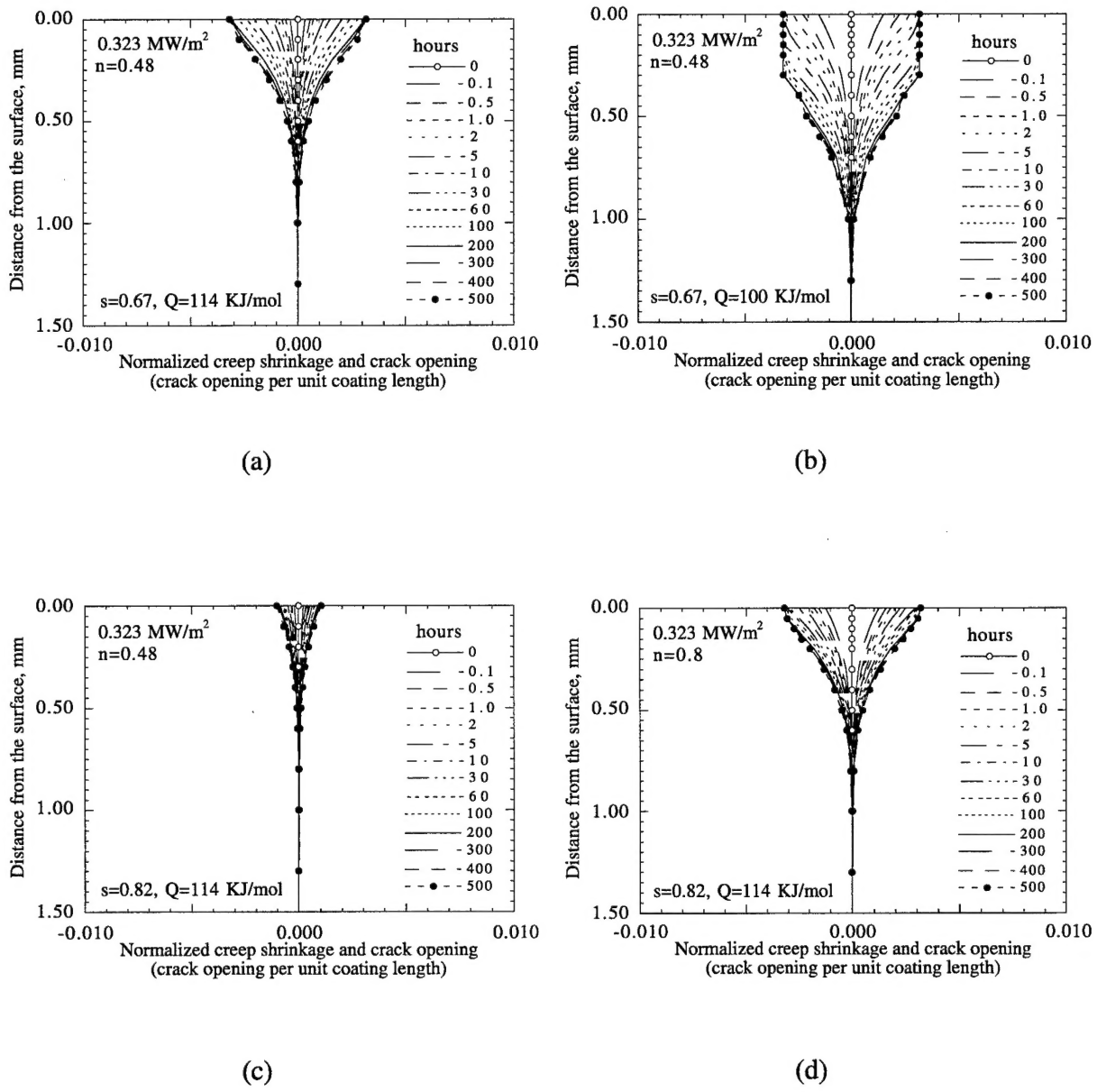

Fig. 2 Simulated coating shrinkage induced cracking showing the influence of coating creep behavior (assumed constant ceramic modulus $E_c = 27.6\ MPa$, ceramic surface temperature 872°C, n stress exponent, s time exponent, and Q activation energy) on the kinetics of the crack opening displacement and penetration depth.

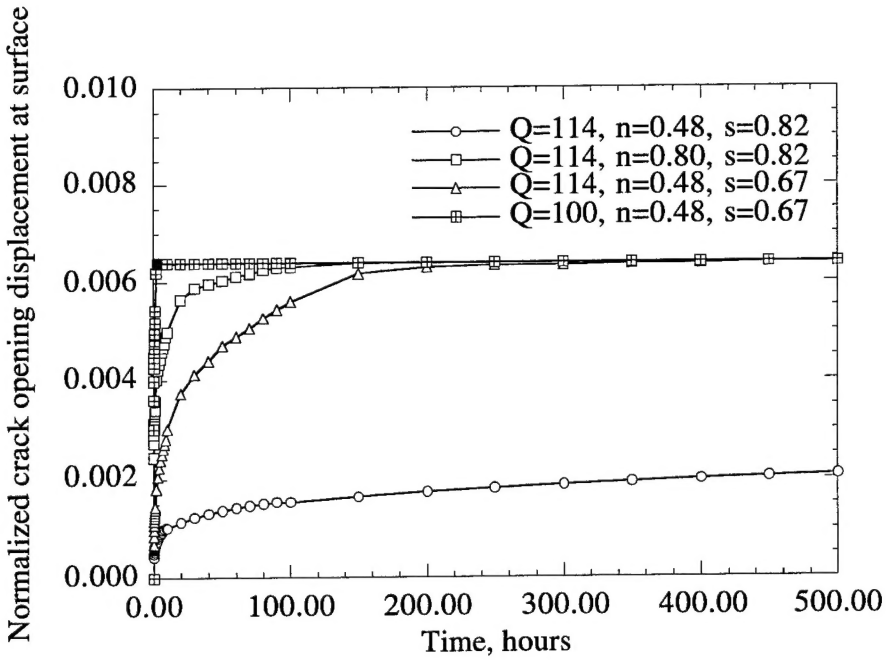

(a)

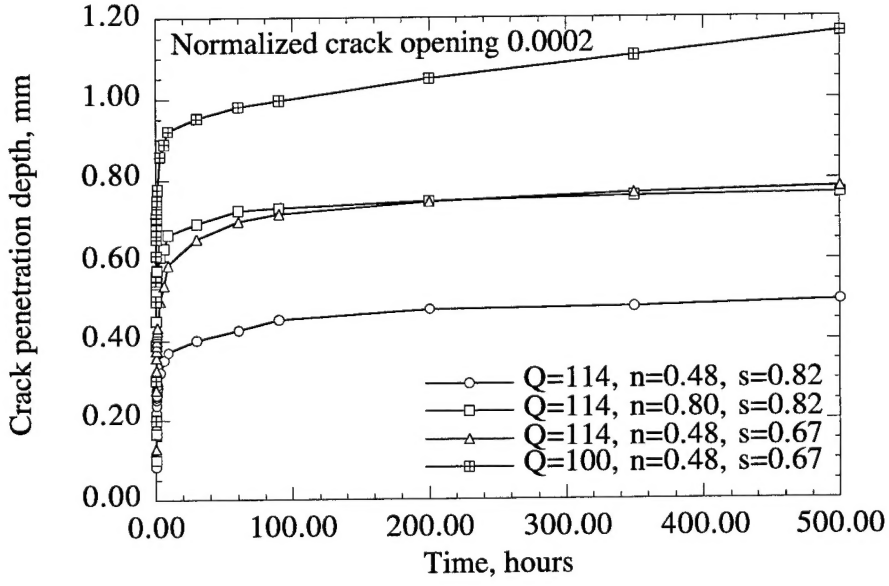

(b)

Fig. 3 The influence of coating creep behavior on crack opening and penetration kinetics (coating thickness 1.6 mm, laser heat flux 0.323 MW/m^2, ceramic surface temperature 872°C). (a) The crack opening at the ceramic surface as a function of laser heating time; (b) The crack penetration depth as a function of laser heating time.

Approach for Constructing the Coating Creep Constitutive Equation

In the laser sintering/creep experiments, the creep strains due to thermally induced stresses in the coating are derived from the crack opening displacements at various coating depths after cooling, as a function of time from several specimens. Because of cracked nature of the coating, the residual in-plane macro-elastic stress, and thus the residual elastic strains, acting on these segments are considered to be zero in the thick ceramic coating after cooling. The bond coat and the substrate creep can be neglected at these low interfacial temperatures. Therefore, the measured crack opening per unit length will only correspond to the ceramic creep strains. The actual creep strain rates in the coating can be determined from the experiments by taking the derivative of the measured creep strain-time curves.

The temperature profiles in the coating system can be determined from the measured ceramic surface and metal substrate temperatures, the coating thicknesses and conductivities of the coating systems. The thermal stresses in the coating system imposed by laser heating can be calculated, as described in Appendix B. Should the stress relaxation in the ceramic coating not occur, the creep constitutive equation could be established readily according to Equation (1) by solving for the constants from the experimental data. However, considerable stress relaxation in the ceramic coating is expected to take place during laser testing. The general approach, for taking stress relaxation into account, may be derived directly from the variable strain rate functions with respect to time and temperature. This variable strain rate change approach is effective in separating the intrinsic creep strain rates and stress relaxation rates from the total measured strain rate changes with respect to time and temperature. From Equation (2), by taking natural logarithm and derivatives with respect to time and temperature, the strain rate changes with respect to time and temperature can be expressed as

$$\frac{\partial \ln \dot{\varepsilon}_p^i(T,t)}{\partial t} = n \cdot \frac{\partial \ln\left[\sigma_0(T) - \varepsilon_p^{i-1}(T,t)\frac{E_c}{1-\nu_c}\right]}{\partial t} - \frac{s}{t} \tag{4}$$

$$\frac{\partial \ln \dot{\varepsilon}_p^i(T,t)}{\partial T} = n \cdot \frac{\partial \ln\left[\sigma_0(T) - \varepsilon_p^{i-1}(T,t)\frac{E_c}{1-\nu_c}\right]}{\partial T} + \frac{Q}{RT^2} \tag{5}$$

where n, s, and Q are constants described above that are to be determined in the creep constitutive Equation (2). The left hand sides of Equations (4) and (5) are the measured strain rate changes with respect to time and temperature, and the right hand sides describe the effects of elastic stress

relaxation, as well as the intrinsic creep time exponent s and activation energy Q, on creep strain rates.

The measured strain rate change with time can be plotted vs. $1/t$. It can be seen that, from Equation (4), in the absence of stress relaxation (or if the creep strain were much smaller than the elastic strain at lower heating temperatures), the slope of $\partial \ln \dot{\varepsilon}_p^i(T,t)/\partial t$ vs. $1/t$ simply gives the time exponent s. As shown in Figure 4 (a) which represents a modeled coating case, the slope of $\partial \ln \dot{\varepsilon}_p^i(T,t)/\partial t$ vs. $1/t$ decreases with increasing depth from the surface (thus with decreasing temperature), and it approaches s towards the inner layer.

The extent of surface stress relaxation, coupled with the differential strain rate change with respect to time between the surface and inner layers in the coating, provides information on the stress exponent n. As can be seen from Equation (4), the stress component can be determined from the measured differential strain rate change, and the surface stress relaxation rate. The stress relaxation rate can be readily determined from the initial elastic stresses that are calculated from the thermal stress analysis in the coating system, and the total accumulated creep strains that are measured experimentally. Figure 4 (a) illustrates the relationship between the strain rate change with respect to time t and the stress relaxation in the coating system.

From Equation (5), it can be seen that the creep activation energy Q can be determined by the measured strain rate change and stress relaxation with respect to temperature. In another words, the strain rate change due to the stress relaxation contribution should also be subtracted from the measured total strain rate change data $\partial \ln \dot{\varepsilon}_p^i(T,t)/\partial T$. As shown in Figure 4 (b), by plotting the strain rate change with respect to temperature (thus to coating depth) as a function of $1/T^2$, the activation energy Q can be obtained from the slopes of the measured strain rate change curve and the stress relaxation curve, provided that the stress exponent n is known.

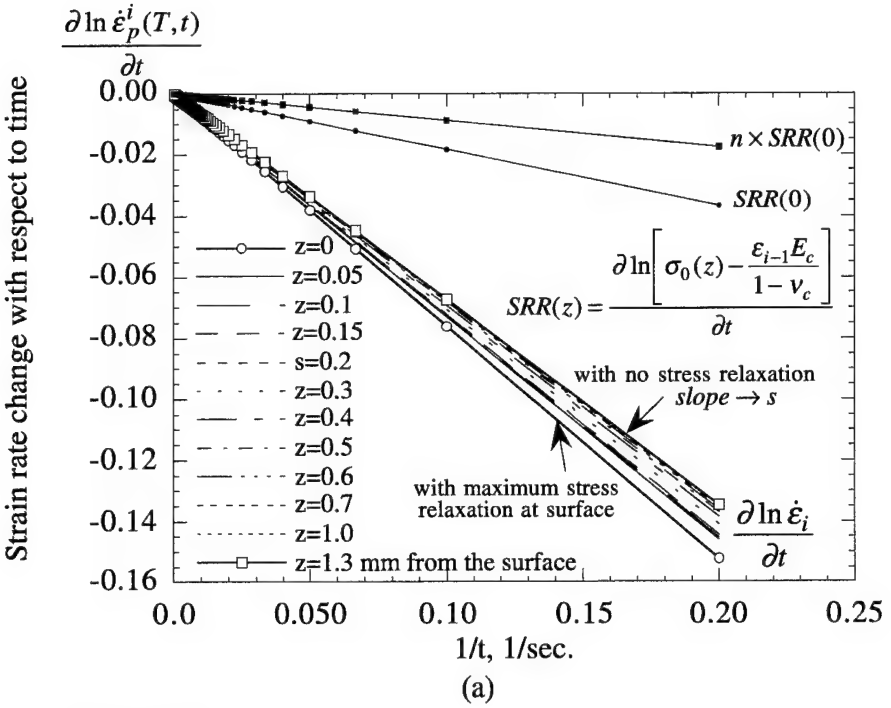

(a)

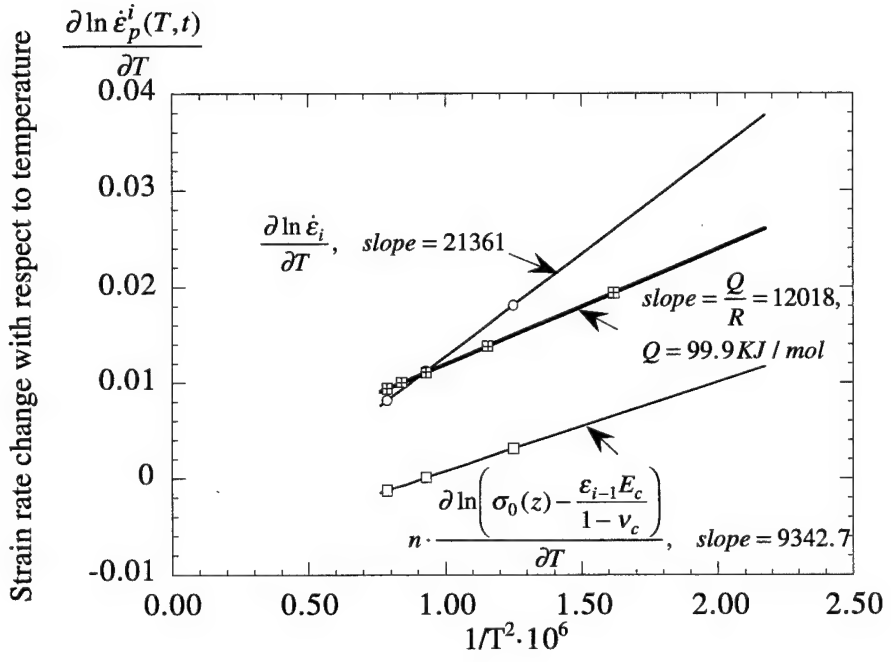

(b)

Fig. 4 Determination of coating creep constitutive equation by laser sintering technique in a simulated coating system (creep activation energy modeled as Q=100 KJ/mol, stress exponent n=0.48 and time exponent s=0.67, *SRR* denotes stress relaxation rate with respect to time). The material creep constants can be obtained by Equations (4) and (5). (a) Strain rate change with respect to time t as a function of $1/t$; (b) Strain rate change with respect to temperature as a function of $1/T^2$.

Elastic Modulus Evolution of the Ceramic Coatings and Variable Modulus Creep Rate Equations

For ceramic coatings with relatively high porosity such as plasma sprayed ZrO_2-Y_2O_3 coatings, the elastic modulus is expected to increase considerably with laser heating time. The modulus change kinetics, which are closely related to coating porosity reduction due to sintering, are greatly affected by the applied compressive stress and the test temperature [18] . The modulus change under the temperature and stress activated conditions can be considered as a relaxation process. A reasonable expression for such a process is

$$\frac{E_c^{\infty} - E_c}{E_c^{\infty} - E_c^0} = \exp\left[-\frac{t}{\tau}\right] \tag{6a}$$

or equivalently

$$\frac{E_c - E_c^0}{E_c^{\infty} - E_c^0} = 1 - \exp\left[-\frac{t}{\tau}\right] \tag{6b}$$

where E_c^0 and E_c^{∞} are ceramic coating modulus values at the initial time and at infinitely long time, respectively, τ is relaxation time in seconds, which can be expressed as a function of temperature and applied stress. This creep and densification in thermal barrier coatings are not only associated with thermally and stress activated diffusion processes, but also related to a mechanical compacting process. Based on these considerations, therefore, τ has been fitted approximately to a temperature and stress function in the present study, from available coating modulus data reported in the literature [18] . The relaxation time τ for a plasma-sprayed ZrO_2-8wt.%Y_2O_3 can be expressed as

$$\tau = \left[\frac{5.5934\times10^{-3}}{T} - \frac{3.0135\times10^{-4}\sigma}{T} + 4.2785\times10^{-7}\sigma^{1.109}\right]^{-1} \tag{7}$$

where T is temperature in Kelvin, and σ is the compressive stress in the coating in MPa. The first and second terms in Equation (7) represent the thermally and stress activated contributions, respectively, whereas the third term describes the stress compacting effect. Since the reported data [18] are very limited, parameters obtained for this physical model in Equation (7) may still only qualitatively describe the process. However, the expression is more than adequate for our present needs. The modulus variations with time and temperature at various applied stress levels are plotted in Figure 5 for assumed values of the initial and final models. It can be seen that the coating modulus increases from an initial value to a final value in a period of time, and the modulus change rate increases with increasing temperature and applied stress. Assuming that the ceramic Poisson's ratio remains constant, Equations (4) and (5) can be rewritten with variable modulus as

$$\frac{\partial \ln \dot{\varepsilon}_p^i(T,t)}{\partial t} = n \cdot \left\{ \frac{\partial \ln\left[E_c(t,T,\sigma)\right]}{\partial t} + \frac{\partial \ln\left[\varepsilon_e^0(T) - \varepsilon_p^{i-1}(T,t)\right]}{\partial t} \right\} - \frac{s}{t} \tag{8}$$

$$\frac{\partial \ln \dot{\varepsilon}_p^i(T,t)}{\partial T} = n \cdot \left\{ \frac{\partial \ln\left[E_c(t,T,\sigma)\right]}{\partial T} + \frac{\partial \ln\left[\varepsilon_e^0(T) - \varepsilon_p^{i-1}(T,t)\right]}{\partial T} \right\} + \frac{Q}{RT^2} \tag{9}$$

where $\varepsilon_e^0(t,T)$ is the initial elastic strain in the coating. Equations (8) and (9) demonstrate that the measured strain rate changes with respect to time and temperature are affected not only by the creep constants s and T, but the modulus and elastic strain relaxation terms as well. From Equation (8) it can be seen that the observed strain rate change with respect to time will be smaller when stress relaxation occurs. The two competing factors, that is, the modulus increase and the elastic strain decrease with time, will respectively enhance and impede the creep strain rate change in the coating. On the other hand, from Equation (9) it can be seen that both modulus term and elastic strain term will facilitate the strain rate change with respect to temperature across the coating. For the both cases described in Equations (8) and (9), however, the elastic strain relaxation terms usually become predominant for longer testing time, as compared to the modulus terms, since the coating modulus saturates to the final value in a relatively short time especially near the surface region.

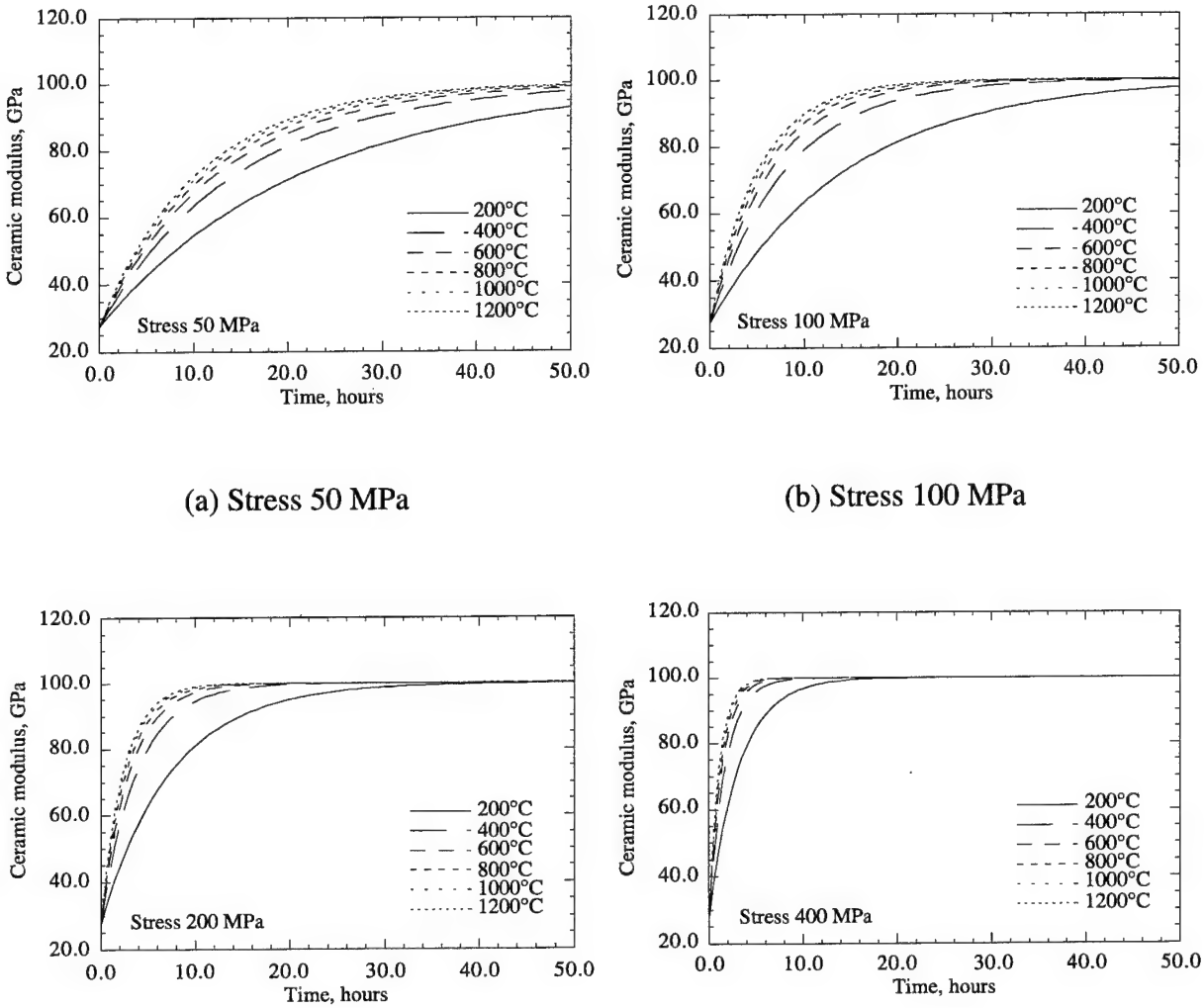

(a) Stress 50 MPa

(b) Stress 100 MPa

(c) Stress 200 MPa

(d) Stress 400 MPa

Fig. 5 Ceramic coating elastic modulus variation as a function of time, temperature and applied stress modeled from Equations (6) and (7). The initial and final modulus values are assumed to be 27.6 GPa and 100 GPa, respectively. The modulus changing kinetics were extrapolated from the available experimental data as described in the text.

EXPERIMENTAL MATERIALS AND METHODS

A thermal barrier coating system, consisting of a ZrO_2-8wt.%Y_2O_3 ceramic coating and an intermediate Fe-25Cr-5Al-0.5Y bond coat, was plasma-sprayed onto 4140 steel using a plasma spray system and a 6-axis industrial robot. The plasma spray conditions used for both the ceramic coating and bond coat have been given previously [8] . The ceramic top coat had approximately 9% porosity after processing. The ceramic coating and bond coat thicknesses were 1.6 mm and 0.25 mm, respectively. The substrate configuration used was 4140 steel rectangular bar with dimension 127×32×12.7 mm.

The laser sintering and creep tests were conducted using a high power 1.5 KW CO_2 laser (EVERLASE, Coherent General Inc., Massachusetts). In order to produce a lower power density and more uniform energy distribution, a Plano Concave ZeSe lens with a focal length -330 mm was used to expand the laser beam. A continuous wave laser beam thus obtained (about 200 watt Gaussian beam) was used to heat a 32 mm diameter area (the Gaussian beam radius is defined as the distance at which the laser power density has dropped to 13.5% of its value at the center) on the ceramic surface [8] , as illustrated in Figure 6. Backside air cooling was used to establish the steep temperature gradient across the coating system. During the laser testing, the specimen surface temperature was measured by an 8 micron infrared pyrometer (Model MX-M803 Maxline Infrared Thermometer Measurement and Control System, Ircon, Inc., Illinois), while the backside metal temperature was determined by a type-R thermocouple. All temperature data were continuously recorded throughout each test. In the laser beam center area, the ceramic surface temperature was maintained at about 1080°C and the back side metal temperature at 100°C. The specimens were continuously heated for either 1 hour, 11 hours, 22 hours or 120 hours. The creep strains near the laser beam center area were measured both on the coating surface and the cross-sections by metallography after cooling. The coating creep time exponent s, stress exponent n and activation energy Q were determined by the variable strain rate change method described above. The constant A was then obtained from the experimental data using the finite difference method described in Appendix C. Note that for the case of constant modulus the constant A may also be obtained from a non-linear regression technique.

During the laser testing, the ceramic coating experiences very complex creep and stress relaxation processes. The creep strain, elastic stress, modulus value, thermal conductivity and temperature in the ceramic coating are all interrelated. The stress and thus creep strain responses in the coating, as a function of time and coating depth, were simulated using a finite difference approach that is described in detail in Appendix C. This approach used available experimental data to incorporate temperature, and time and/or stress dependent Young's modulus and thermal

conductivity changes into the creep calculations. The modeled results provide insights into the coating creep behavior, and help to better understand the important aspects of coating creep mechanisms under high heat flux conditions.

EXPERIMENTAL RESULTS

The Creep Behavior of the Ceramic Coating

Through-thickness wedge-shape cracks in the ceramic coatings are observed in all specimens after laser sintering and creep tests. Figure 7 shows typical micrographs of the coating surface and cross-sections near the laser beam center region after laser sintering/creep tests. The crack width at the surface, as shown in Figure 7 (a), decreases with increasing the distance from the center due to the temperature profiles imposed by the wide spread Gaussian beam power distribution. From Figure 7 (b) and (c), it can be seen that the overall coating porosity is reduced, especially near the coating surface where the highest temperature and in-plane compressive stress are expected. The porosity is also decreased with increasing laser testing time. The pore number and size, splat boundary density and width slightly decrease with increasing distance from the surface. As revealed in scanning electron microscope (SEM) micrographs in Figure 8, the microcrack density observed in the ceramic coating near the surface region, is much lower than that near the ceramic/bond coat interface region. Also, the microcracks that are perpendicular to the in-plane stress directions are more greatly reduced by the deformation process. Although the porosity gradients across the coating thickness after laser testing are difficult to determine quantitatively, it is believed that the porosity reduction in the coating can more or less be correlated to the measured total creep strain gradients. The morphology change in the ceramic coating is expected to result in coating modulus and thermal conductivity increases with laser testing time. However, the coating conductivity increase in the heat flux direction seems less significant. In this study with the constant heat flux and fixed backside metal temperature, no appreciable temperature increase has been observed during the laser creep testing. This may imply that the overall effective coating thermal conductivity does not change sufficiently under the conditions encountered in this study.

Figure 9 illustrates the creep strain distributions measured after various testing times. Noticeable strains are observed as deep as 1 mm into the coating depth. The creep strains increase rapidly during the initial time, and then increase in a much slower rate for longer testing times. The creep strains also decrease with increasing the distance from the surface, and the coating surface strain reaches about 1.2% after 120 hours. As mentioned, the creep strain gradients, resulting from the temperature and stress gradients imposed by laser heating, dictate the material intrinsic creep properties and provide insights to the coating stress-strain response at temperature.

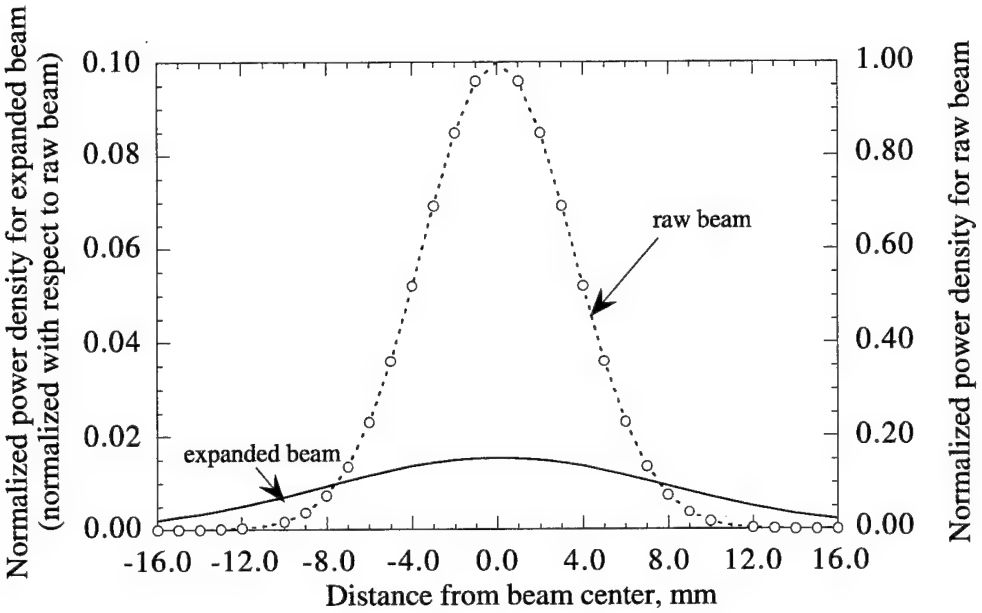

(a)

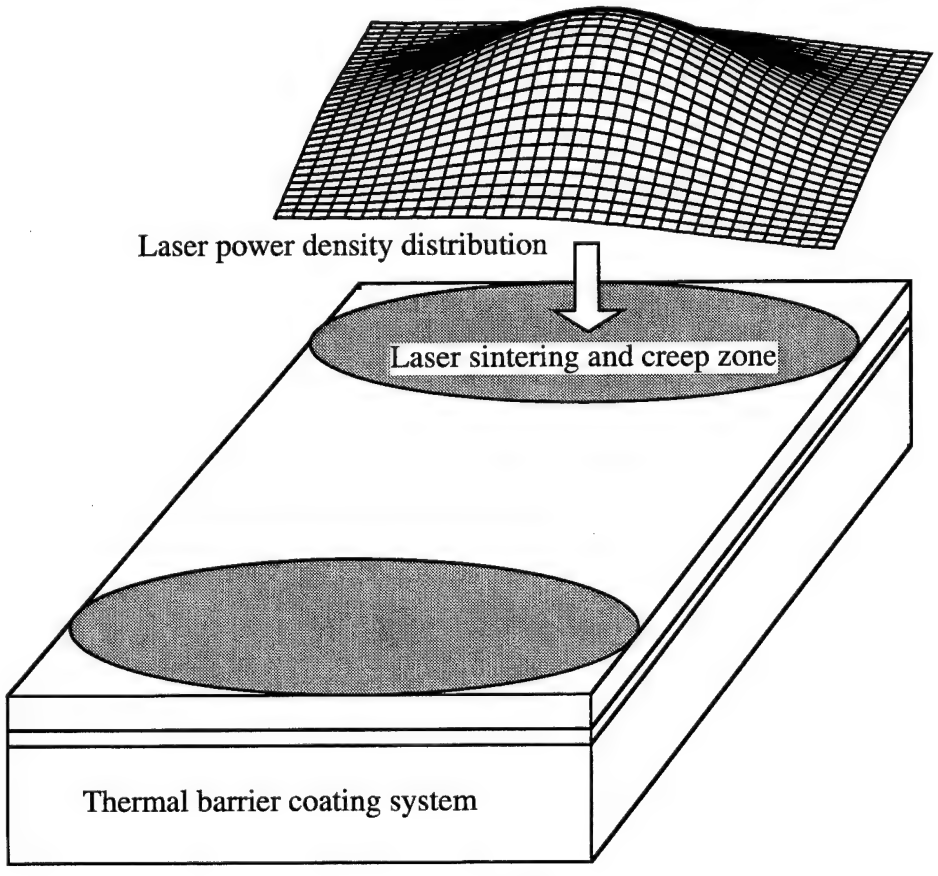

(b)

Fig. 6 Laser sintering and creep experiments for a thermal barrier coating system. (a) Normalized laser beam power distributions for a raw beam and an expanded beam; (b) The expanded laser beam provides more uniform heating over a large area on the specimen surface.

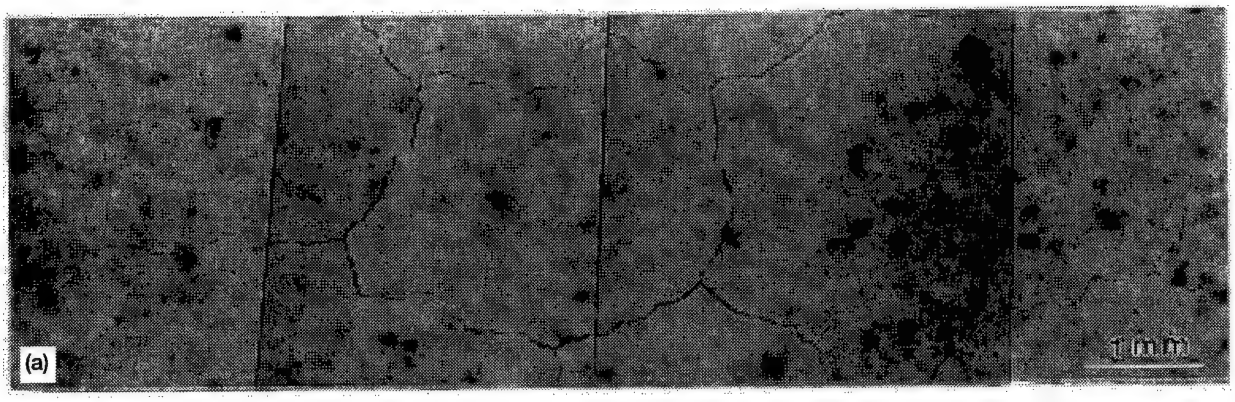

Fig. 7 Optical micrographs of the ceramic coatings after laser sintering/creep tests (the surface and the ceramic/bond coat interface temperatures were about 1080°C and 242°C, respectively). (a) Coating surface morphology showing the equiaxial crack distribution after 11 hour laser testing;

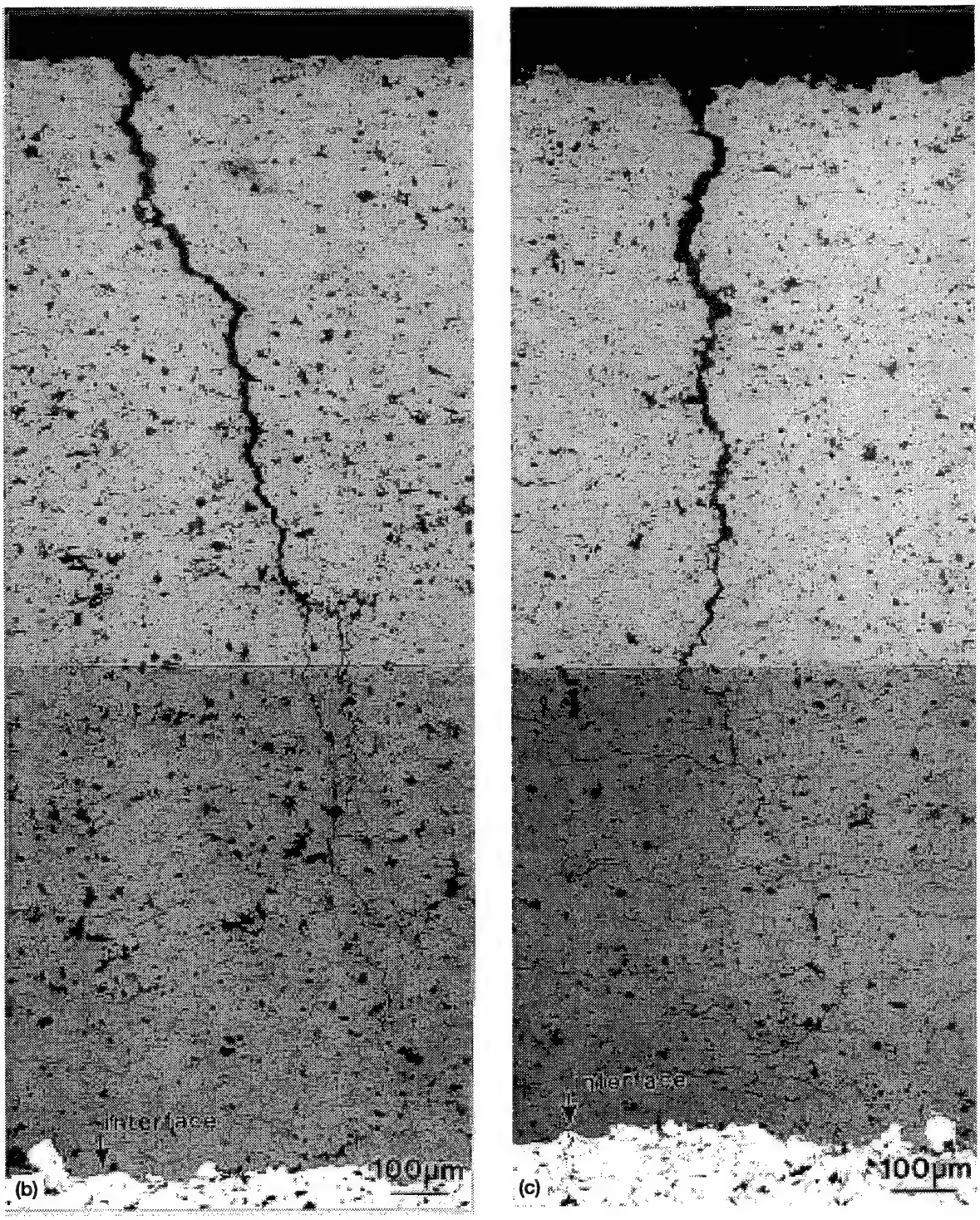

Fig. 7 (Continued). Optical micrographs of the ceramic coatings after laser sintering/creep tests (the surface and the ceramic/bond coat interface temperatures were about 1080°C and 242°C, respectively). (b) and (c) The cross-sections of the ceramic coatings near wedge-shape cracks after 11 hour and 120 hour laser testing, respectively. Porosity change across the coating thickness can also be observed.

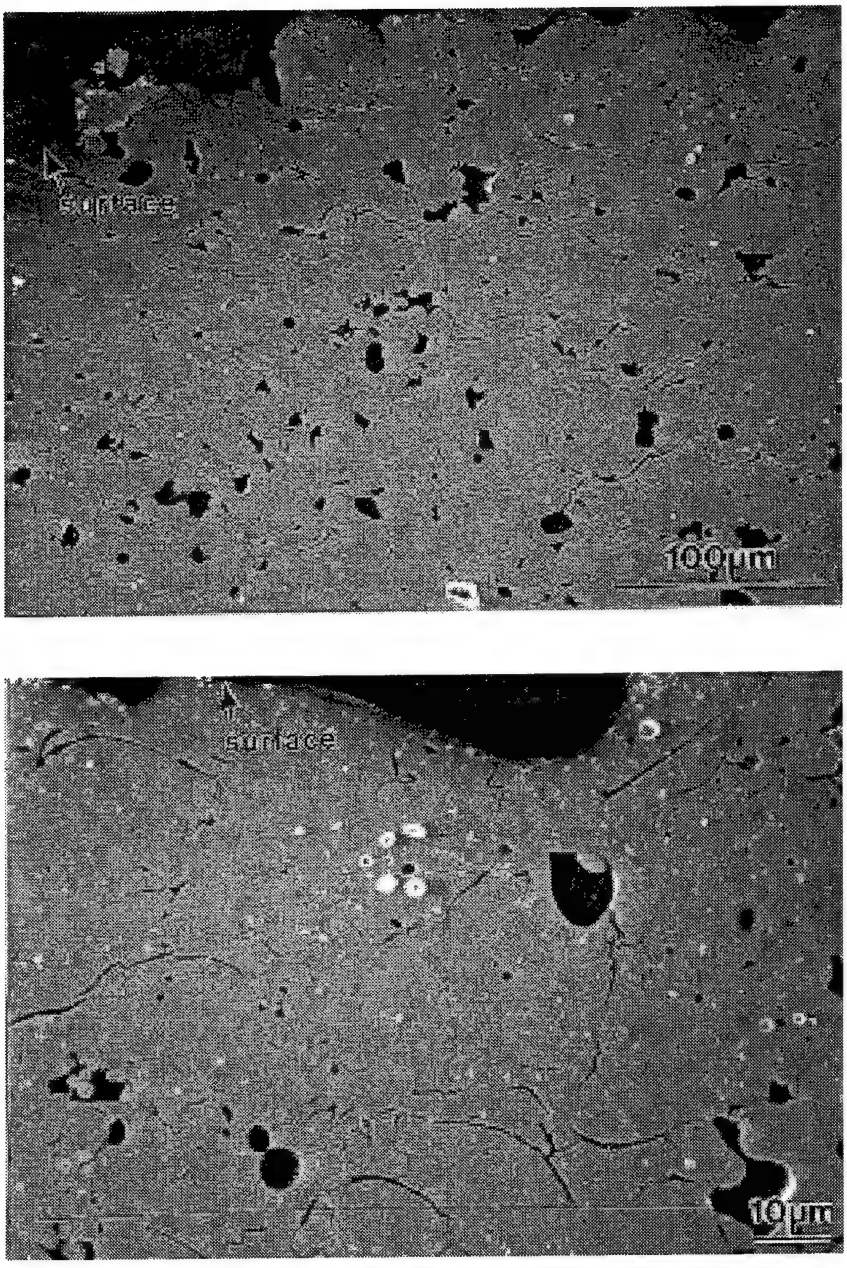

(a)

Fig. 8 SEM micrographs of the cross-sections of the ceramic coating after 120 hour laser testing showing the microcrack morphologies. (a) The ceramic coating near the surface; (b) The ceramic coating near the ceramic/bond coat interface.

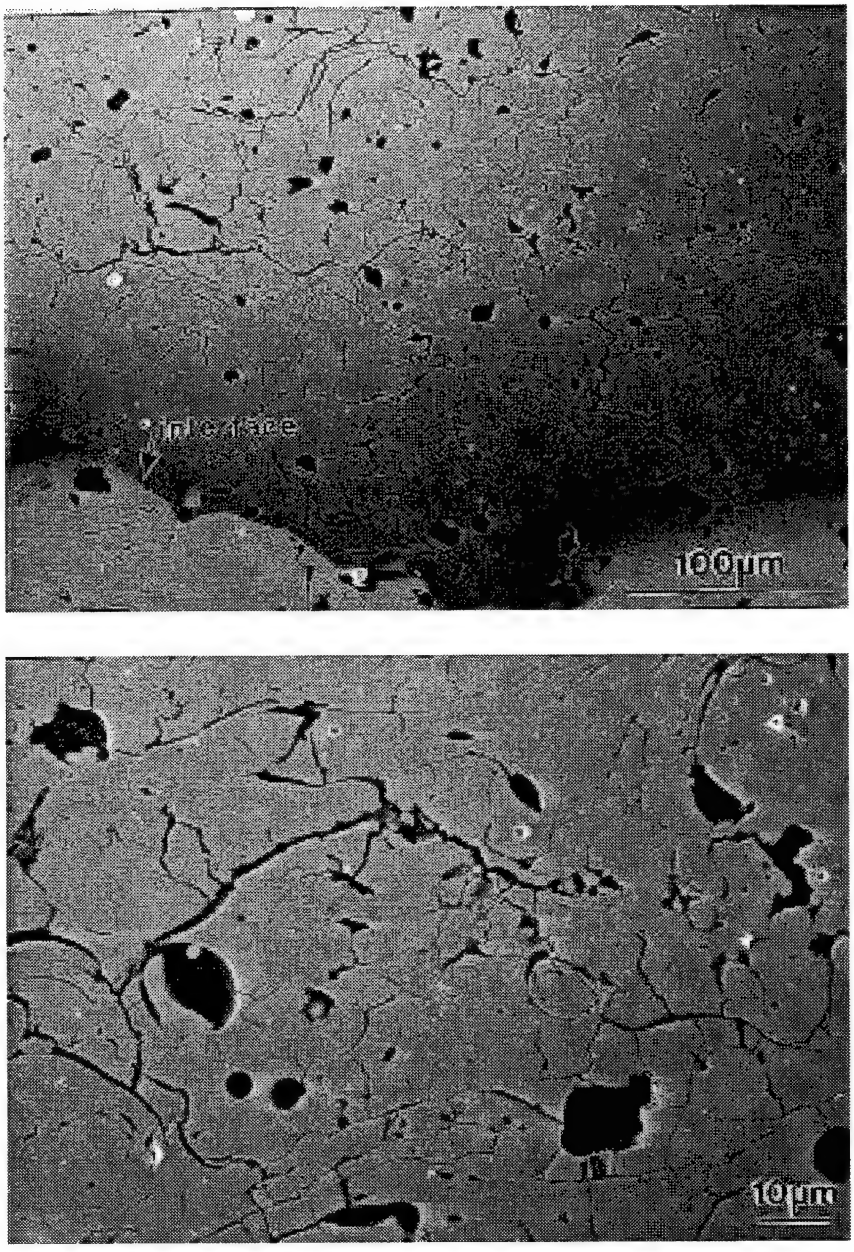

(b)

Fig. 8 (Continued) SEM micrographs of the cross-sections of the ceramic coating after 120 hour laser testing showing the microcrack morphologies. (a) The ceramic coating near the surface; (b) The ceramic coating near the ceramic/bond coat interface.

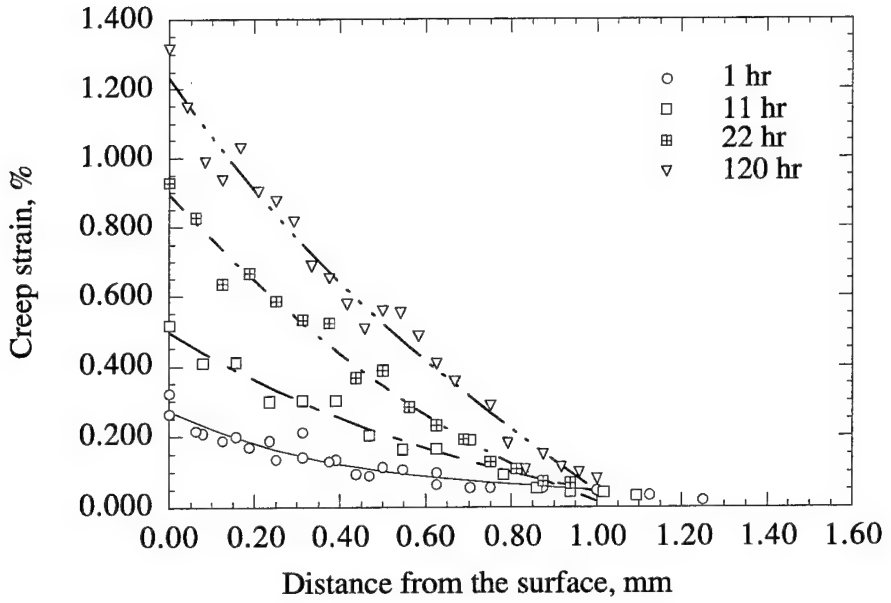

Fig. 9 Creep strain distributions in the ceramic coating after laser sintering and creep tests. The strain gradients are resulting from the temperature and stress gradients imposed by laser heating.

Figure 10 shows the relationship between the creep strain and time at the various coating depths. The experimental data have been fitted in the following forms

$$\dot{\varepsilon}_p(T,t) = A(T)\cdot t^{-s_m} \tag{10a}$$

$$\varepsilon_p(T,t) = \frac{A(T)}{1-s_m}\cdot t^{1-s_m} \tag{10b}$$

where $A(T)$ is a constant depending on temperature, s_m and $1-s_m$ are experimentally measured time exponents for the strain rate and strain equations. It can be seen that, with increasing coating depth and thus with decreasing temperature, the measured time exponent s_m approaches a constant about 0.67. This value is taken as the creep strain rate time exponent s, which is the intrinsic material constant for describing the coating primary creep behavior. The observed higher strain rate time exponent s_m near the surface region is attributed to the extensive stress relaxation in the coating.

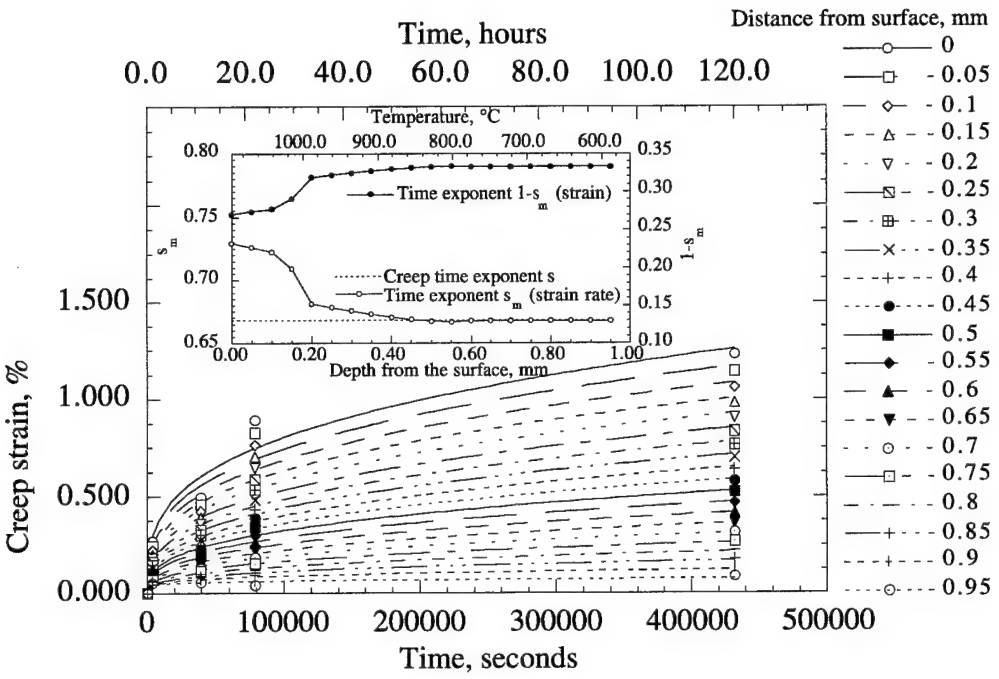

Fig. 10 The relationship between the creep strain and time at the various coating depths. The creep strain in the coating increases with time, but decreases with temperature. The measured strain rate time exponent approaches s in the inner layers of the coating where the temperature is relatively low and stress relaxation rate is less significant.

The stress exponent n and creep activation energy Q can be determined from the experimental data by the variable strain rate approach described earlier in this paper. Since the ceramic coating modulus is expected to change during laser testing, Equations (8) and (9) should be used to solve for these creep constants. However, under the temperature and stress regime of interest, the elastic modulus of the ceramic coating reaches the final value quickly as dictated by Equations (6) and (7). Therefore, the elastic strain relaxation terms in Equations (8) and (9) are predominant for longer testing time so that the modulus terms may be neglected. As a consequence, in the present study the strain data after one hour are used, and the modulus terms in Equations (8) and (9) were neglected for the calculations of stress exponent n and creep activation energy Q. Figure 11 illustrates the measured strain rate changes with respect to time and temperature, as well as the stress relaxation effects. The creep constants obtained from this experiment for the plasma sprayed ZrO_2-8wt.%Y_2O_3 coating are listed in Table 1.

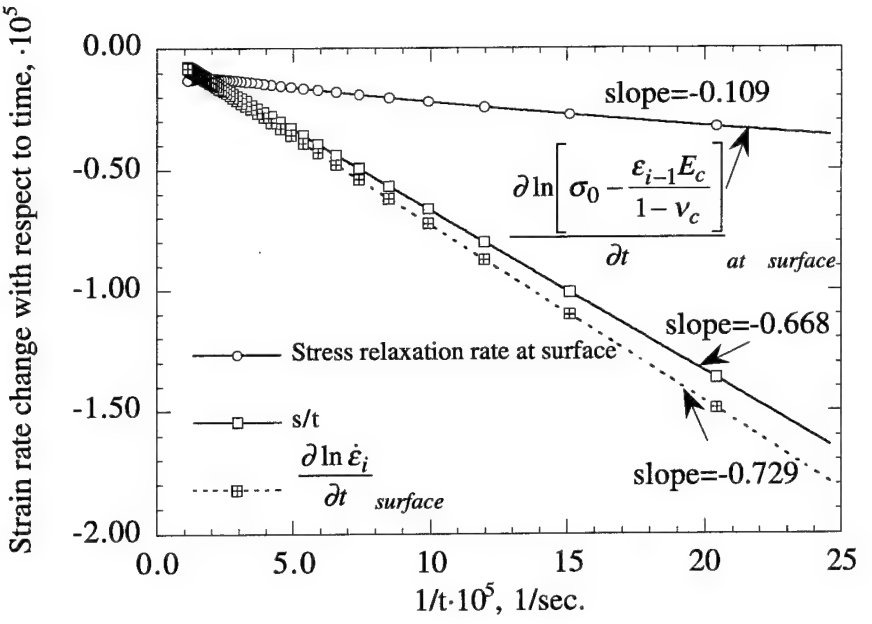

(a)

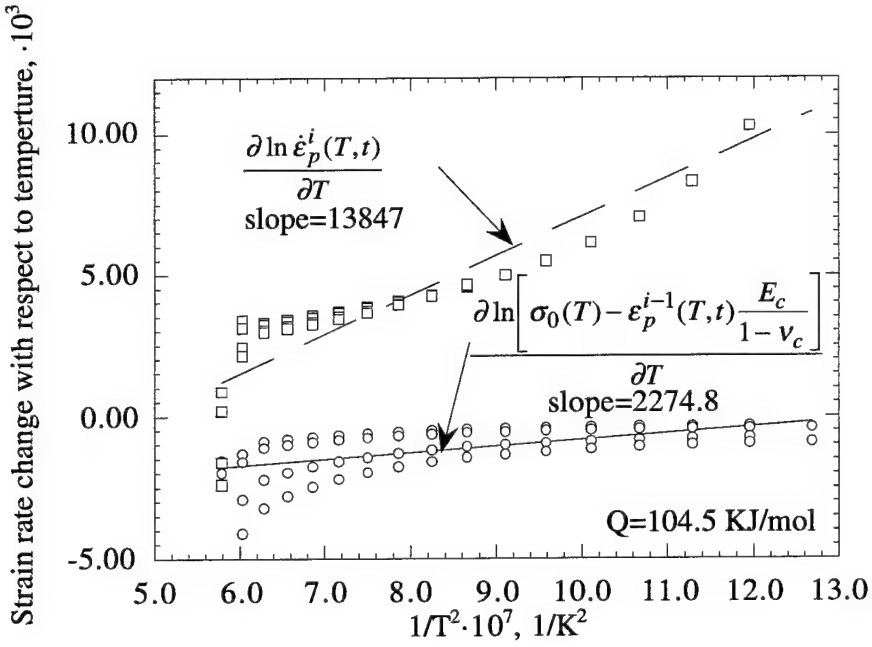

(b)

Fig. 11 Experimental laser creep testing results for a plasma sprayed ZrO_2-8wt.%Y_2O_3 coating. (a) Strain rate change with respect to time t and stress relaxation rate as a function of $1/t$; (b) Strain rate change and stress relaxation with respect to temperature as a function of $1/T^2$.

Table 1. The constants in the creep constitutive equation determined by laser sintering technique for a plasma sprayed ZrO_2-8wt.%Y_2O_3 ceramic coating

Material	Pre-exponent constant A	Time exponent s	Stress exponent n	Activation Energy Q, KJ/mol
Plasma sprayed ZrO_2-8wt.%Y_2O_3	0.026	0.67	0.56	104.5

Simulation of Coating Stress and Creep Strain Responses During Laser Testing

During laser sintering, the thermal elastic stresses in the coating are expected to relax with increasing the creep strain. On the other hand, the coating modulus will increase with increasing time due to the coating densification and creep process. Figure 12 shows the simulated coating elastic modulus and thermal conductivity evolution, as well as the temperature change, with time as predicted by the finite difference calculations (Appendix C) based on the measured coating creep behavior.

As can be seen in Figure 12 (a), the coating modulus near the surface region reaches the assumed final value 100 GPa in about 3 hours. In contrast, the coating modulus near the ceramic/bond coat interface region reaches the final value in about 40 hours, due to the lower temperature and compressive stress in this region.

Thermal conductivity is also expected to increase as a function of time and temperature according to published data for sintered plasma sprayed zirconia [19-21] . To a first approximation, the thermal conductivity change due to sintering under the condition of no external stress can be used for this calculation, because the stress perpendicular to the interface is expected to be low in the present study. The thermal conductivity change kinetics, which may be described by $\ln[k/k_0]$ as a function of the Larson-Miller $(L-M)$ parameter, are strongly dependent on the microstructures of the plasma-sprayed zirconia coatings (where k_0 and k are the thermal conductivity values at the initial time zero and any given time t, respectively, the Larson-Miller parameter is expressed as $L-M=T[\ln(t)+C]$, t is the heating time in seconds and T is the absolute temperature in Kelvin, C is a constant) [21] . The literature [21] reported slope of the $\ln[k/k_0]$ vs. $L-M$ plot for very porous yttria fully-stabilized zirconia is 27×10^{-6}, which is much greater than that for relatively dense yttria partially-stabilized zirconia where the slope is 5.1×10^{-6}. For the present experiments, where the coating consists of yttria partially stabilized zirconia of intermediate porosity, an intermediate value of the slope may be anticipated. Using the high slope

value as an upper limit, a small increase in thermal conductivity near the surface region is obtained, as shown in Figure 12 (b). With the lower slope data a smaller increase in thermal conductivity is predicted at the surface, but the conductivity increases occur much deeper into the coating. The low slope data further predict that conductivity changes would begin to occur at extremely short times which would not be observed experimentally. Therefore either case effectively leads to the prediction of small increases in the overall thermal conductivity of the ceramic coating under the test conditions. As a consequence of this, the temperature profile across the coating remains virtually constant with time, as illustrated in Figure 12 (c).

Figure 13 shows the modeled coating elastic stress evolution and creep strain development as a function of time. From Figure 13 (a), it can be seen that the coating compressive stresses in the inner layers increase with time initially, then maintain approximately constant values for longer times. This stress variation is consistent with the modulus change in the coating for this region. However, the coating stresses in the outer layers reach maximum values during the initial 1 to 3 hours, then decrease significantly with increasing time because considerable stress relaxation occurs due to the coating creep. Figure 13 (b) shows that significant creep strain gradients are generated in the coating by the laser creep test. A much higher creep strain in the surface layer has been obtained as compared with the inner layers. The creep strain rates, as shown in Figure 13 (c), are all decreasing with time, and this behavior is expected for the primary creep stage. The creep rates in the several very surface layers are even lower than those in some more inner layers because of the stress relaxation. The modeled creep behavior is in a good agreement with the experimental measurements.

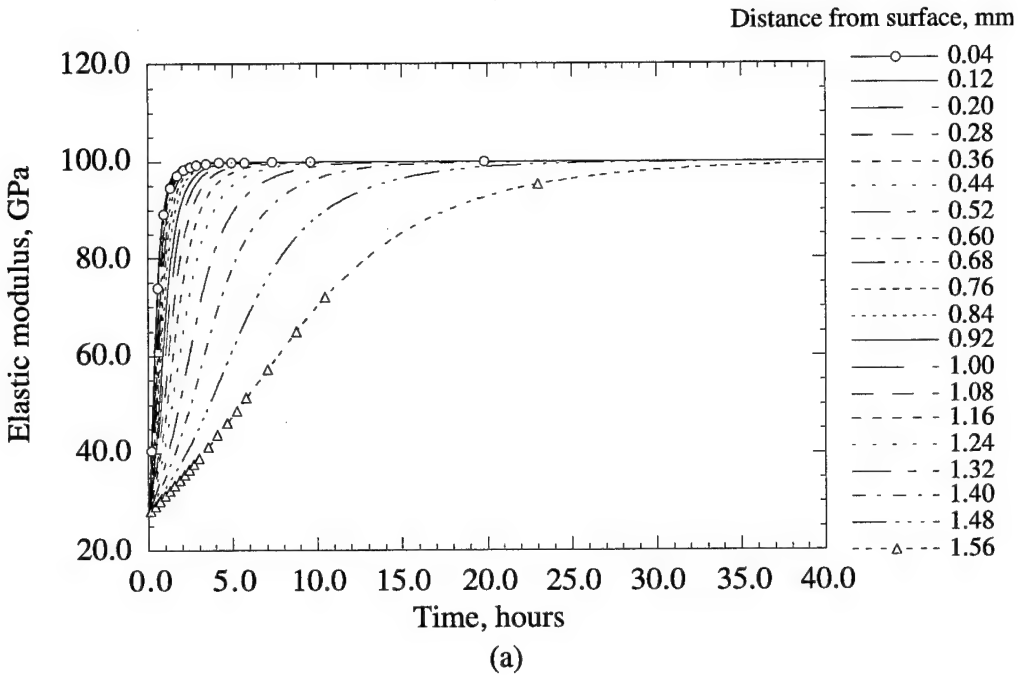

(a)

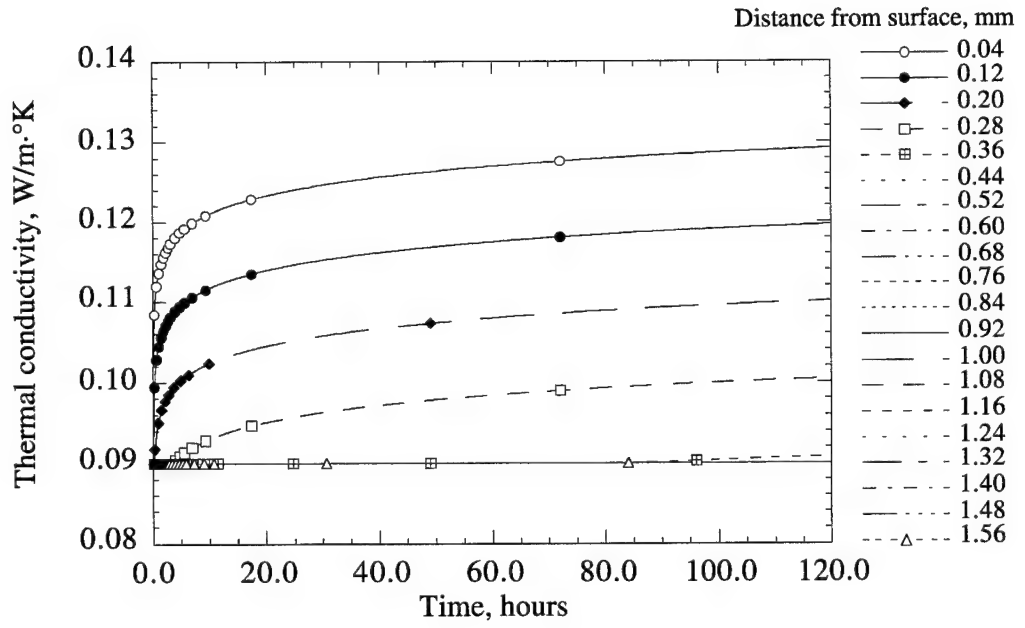

(b)

Fig. 12 Simulated ceramic coating modulus, conductivity and temperature evolution with time at various coating depths, under laser induced temperature and stress conditions. The results are modeled by finite difference approach from the measured ceramic creep behavior, and temperature, time, and/or stress dependencies of the modulus and conductivity. The initial and final values are assumed to be 27.6 GPa and 100 GPa for modulus, and initially 0.9 W/m-K for conductivity, respectively. (a) Ceramic coating modulus as a function of time; (b) Ceramic coating conductivity as a function of time, using the upper limit high slope of the $\ln[k/k_0]$ vs. $L-M$ plot.

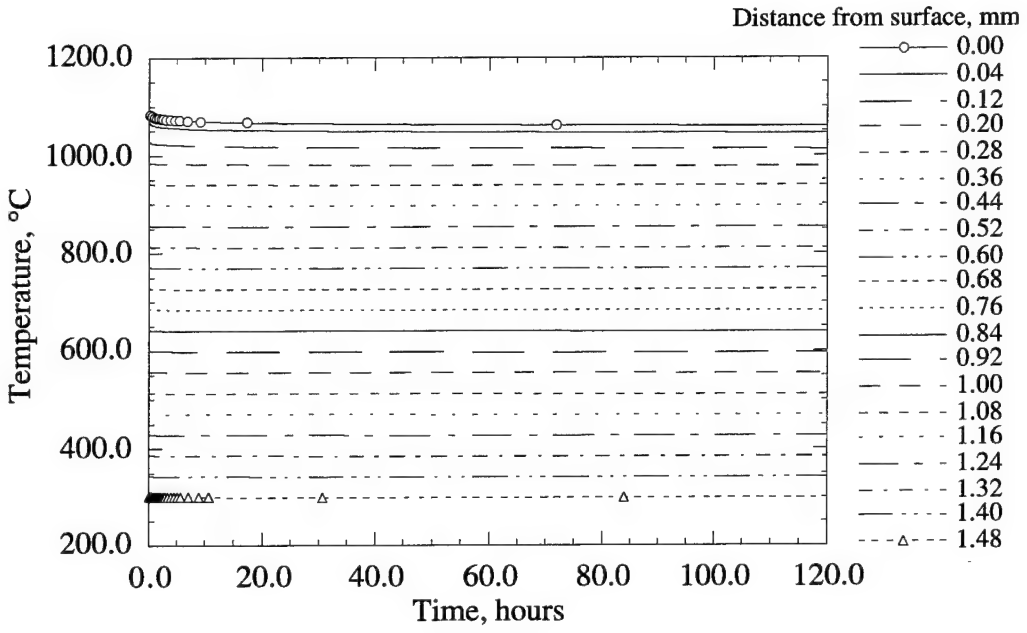

(c)

Fig. 12 (Continued) Simulated ceramic coating modulus, conductivity and temperature evolution with time at various coating depths, under laser induced temperature and stress conditions. The results are modeled by finite difference approach from the measured ceramic creep behavior, and temperature, time, and/or stress dependencies of the modulus and conductivity. The initial and final values are assumed to be 27.6 GPa and 100 GPa for modulus, and initially 0.9 W/m-K for conductivity, respectively. (c) Ceramic coating temperature as a function of time.

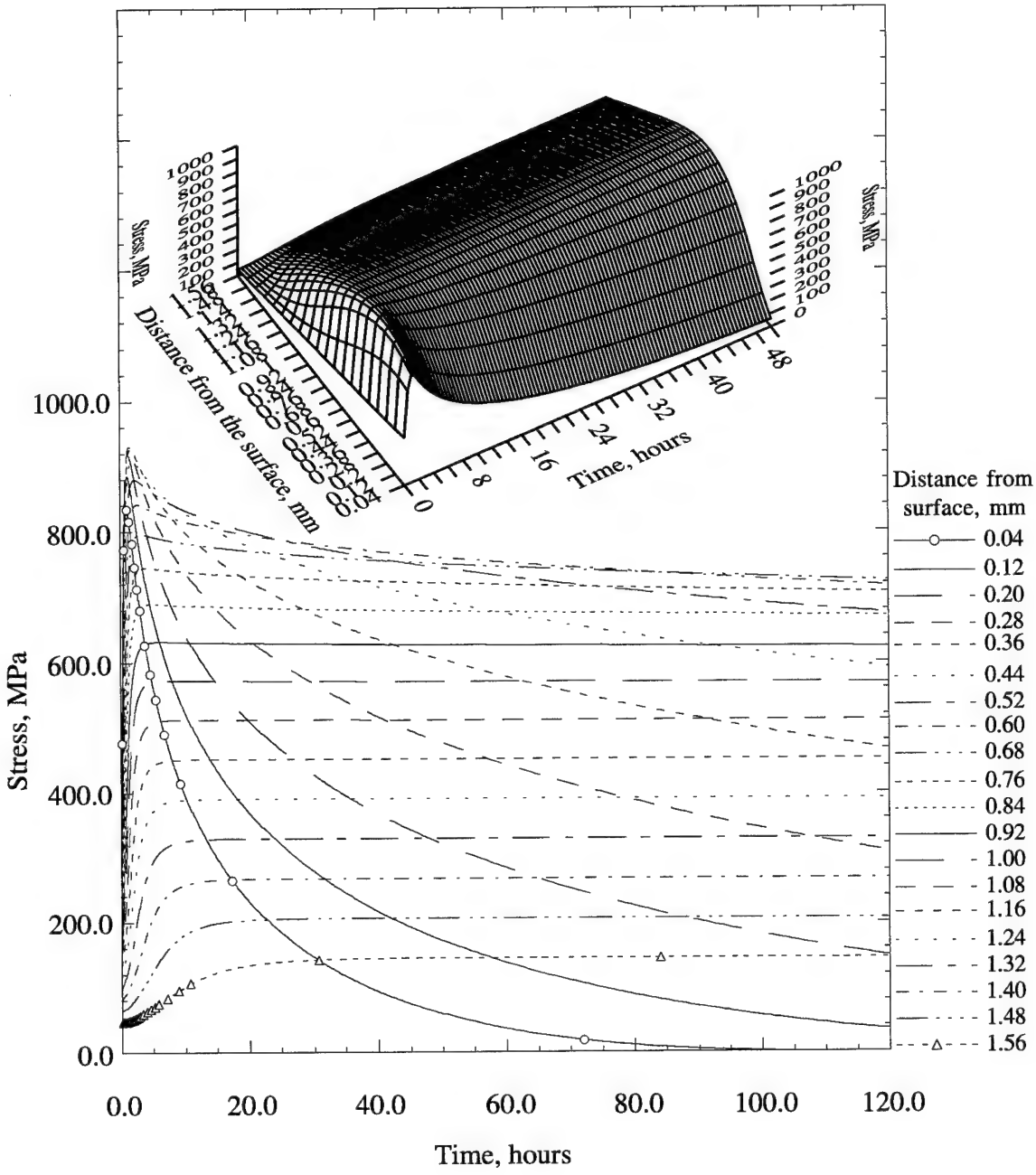

(a)

Fig. 13 The modeled coating stress, total creep strain and creep rate as a function of time and coating depth. Near the surface high initial stress and temperature region, significant stress relaxation and large creep strains are observed. (a) Coating stress as a function of time (The data for the first 50 hours are also presented in a time—coating depth—stress 3 dimensional insert);

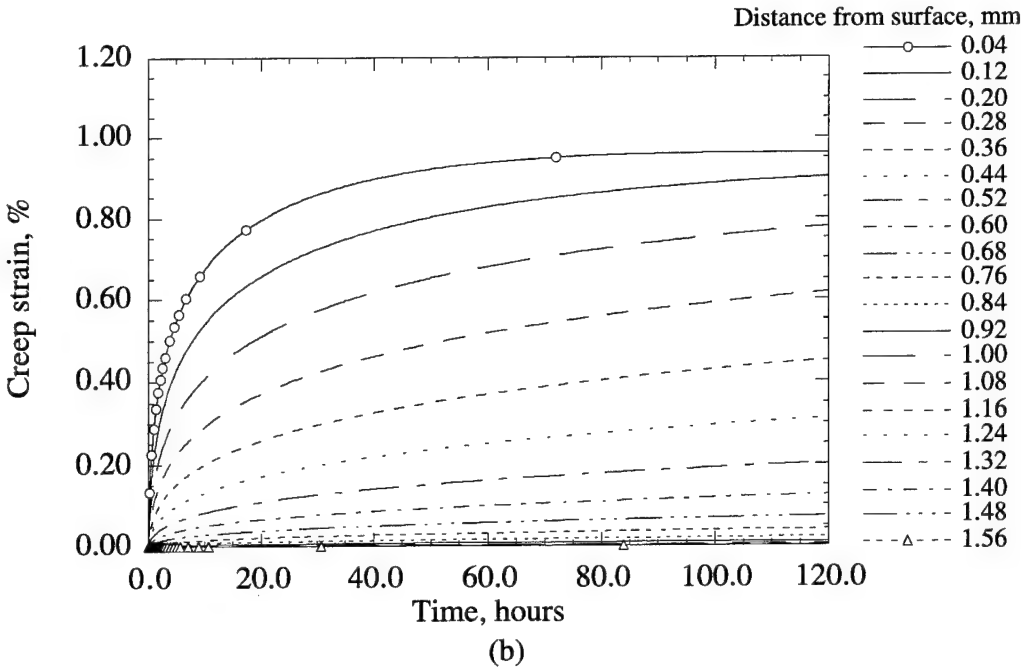

(b)

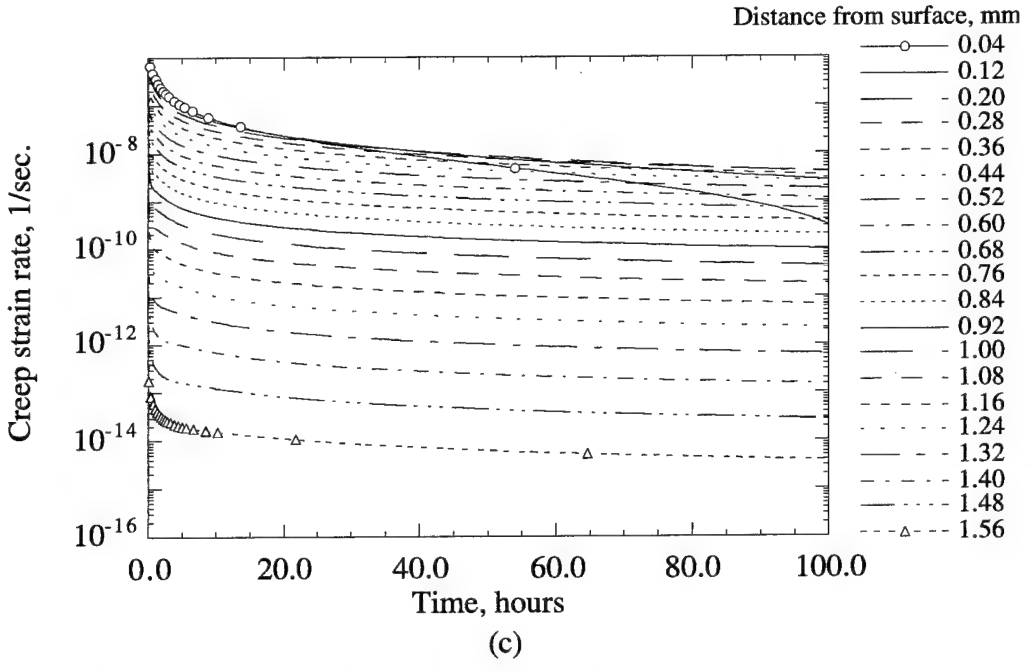

(c)

Fig. 13 (Continued). The modeled coating stress, total creep strain and creep rate as a function of time and coating depth. Near the surface high initial stress and temperature region, significant stress relaxation and large creep strains are observed. (b) Coating creep strain as a function of time; (c) Creep strain rate as a function of time.

DISCUSSION

The laser sintering and creep technique discussed in this paper offers a unique approach for quantitatively determining the ceramic coating pressure sintering and creep behavior under high heat flux conditions. Compared with the conventional creep test, this method is characterized by relatively high compressive stress capability, high strain measurement sensitivity, stress and temperature gradients representative of in-service conditions, as well as potentially high reproducibility and reliability. It is also especially suitable for the coating creep ranking tests that are aimed at developing creep resistant high performance ceramic coatings. The coating modulus and thermal conductivity changes with time can also be incorporated and verified in these tests, from the observed stress relaxation phenomena, creep strain evolution and temperature variation during testing.

The small change in the ceramic surface temperature observed during the laser testing implies little change in overall coating thermal conductivity. This is in sharp contrast to the predicted behavior of the elastic modulus, where the modulus is believed to have increased dramatically in a relatively short time period throughout the coating. We postulate that this difference arises because high in-plane stresses have a strong effect on the modulus, whereas the conductivity is mostly influenced by stress perpendicular to the interface where the stresses are expected to be low. The splat boundaries parallel to the interface throughout most of the coating thickness remained the original as-sprayed characteristics, so effective thermal conductivity would change little except near the surface region where slight increase in the conductivity is expected, as modeled in the finite difference calculations. Thus, the temperature will remain nearly constant through the testing in the coating system, as shown in Figure 12 (c).

The creep characteristics of the ZrO_2-8wt.%Y_2O_3 ceramic coating, determined by the laser creep technique, are consistent with the results obtained from high temperature mechanical fatigue tests [22] and creep tests [10, 15] . The measured creep behavior of the ceramic coating in this study also demonstrates several important issues concerning the thermal barrier coating durability. The significant primary creep stage, as described by time exponent s, could be critical to coating life. The relatively low activation energy Q suggests that the creep and sintering effect could occur deep in the coating even where the temperature is expected to be low. The low stress exponent n may indicate the relatively weak and porous nature, as well as the strong sintering effect, of the coating.

The deformation mechanisms for plasma-sprayed thermal barrier coatings are complex. Figure 14 shows a schematic diagram of proposed ceramic coating creep mechanisms. The

coating creep deformation could be accomplished by stress induced mechanical sliding, as well as thermally and stress activated diffusion process. The large primary creep strains developed in the coating and the low stress exponent may, at least in part, be attributed to the mechanical sliding along the splat boundaries. The porous and weak ceramic coating could cause local stress concentration and redistribution around the micro cracks and splat boundaries, thus significant creep strains could develop even at low nominal stresses. The creep phenomenon in the coating involves a great portion of mechanical compaction and sintering processes that would not require significant stress increase for further deformation.

Creep deformation of ceramics usually requires diffusion of the cations and anions in these materials. Experiments [16, 23, 24] have shown that the creep activation energy is consistent with diffusion activation energies of the ions, depending on the rate limiting steps. In general, creep in compounds occurs in such a way that the rate is determined by the slowest constituent, since complete lattice molecules have to be displaced and the various constituent fluxes are coupled in order to maintain the overall composition of the materials [25] . The creep rate in ceramics is thus determined by the diffusion of the slowest species, diffusing along the fastest path. In yttria stabilized zirconia, the majority defect types are oxygen vacancies $V_O^{\cdot\cdot}$ and yttrium aliovalent dopants at normal cation sites $Y_{Zr}^{'}$. The possible minority defects are zirconium vacancies $V_{Zr}^{''''}$, zirconia interstitials $Zr_i^{\cdot\cdot\cdot\cdot}$ and yttrium interstitials $Y_i^{\cdot\cdot\cdot}$ [26] . The zirconium and yttrium cation transport is confirmed to be the slowest process at least in yttria stabilized zirconia single crystals. The measured cation diffusion activation energies are 461 KJ/mol, 462 KJ/mol for zirconium and yttrium cations, and 86 KJ/mol for oxygen anions, respectively [26] . The reported creep activation energy for yttria stabilized zirconia, however, is in the range of 369 to 657 KJ/mol, depending on the operating creep mechanisms [23, 27, 28]. Considering that cation diffusion is believed to be the rate limiting step, the experimentally measured creep activation energy in this study for the plasma sprayed ZrO_2-8wt.%Y_2O_3 coating is significantly lower as compared to the fully dense yttria stabilized zirconia. Mechanical sliding, fast surface and grain boundary diffusion, and temperature and stress gradient enhanced transport are several possible mechanisms for explaining the experimental phenomena. In addition, for extremely rapid diffusion paths such as splat boundaries, the anion diffusion may become the rate limiting step, and the cation and anion fluxes may be decoupled for the highly nonstoichiometric oxide through formation or annihilation of the oxygen defects in these regions. By incorporating thermally activated and stress enhanced diffusion into the creep constitutive law, Equation (1) can be modified as

$$\dot{\varepsilon}_p = A \cdot \exp\left(-\frac{Q}{RT}\right) \cdot \sigma^n \cdot t^{-s} = A \cdot \exp\left(-\frac{Q_D}{RT} + \frac{\sigma_{local} \Delta V_i}{RT}\right) \cdot \sigma^n \cdot t^{-s} \qquad (11)$$

where Q is the apparent creep activation energy measured in the experiments, Q_D is the diffusion activation energy including all contributions from lattice, grain boundary and surface diffusions, ΔV_i is the molar volume change due to the defect formation, and σ_{local} is the locally concentrated stresses in the coating. From Equation (11), it can be seen that the stress enhanced diffusion can significantly reduce the apparent creep activation energy. Further research may be necessary to identify the important processes concerning the coating sintering, deformation and creep behavior.

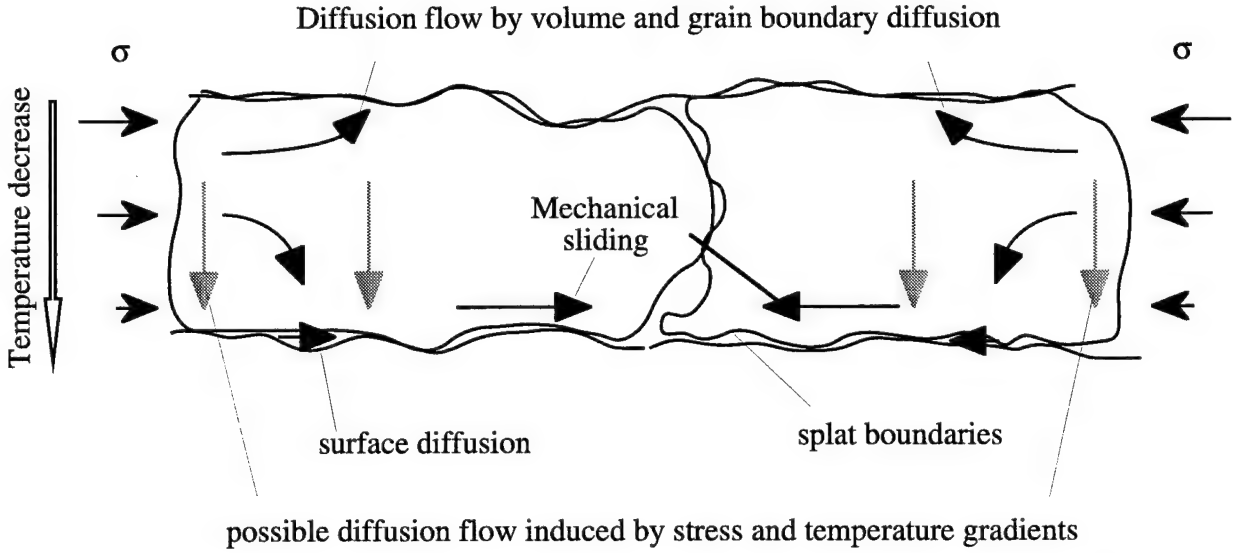

Fig. 14 Schematic diagram showing possible creep mechanisms in a plasma sprayed ceramic coating under laser imposed temperature and stress gradients.

CONCLUSIONS

1. A laser-based creep sintering technique has been proposed for quantitatively evaluating ceramic creep behavior under simulated high heat flux engine conditions. This approach may be promising for coating design and development, stress modeling, and life prediction for various thermal barrier coating applications.

2. The constitutive creep equation for a plasma sprayed ZrO_2-8wt.%Y_2O_3 ceramic coating has been established in these preliminary experiments. The significant primary creep stage and low activation energy observed are attributed to stress induced mechanical sliding, and temperature and stress enhanced cation diffusion through splat and grain boundaries.

ACKNOWLEDGMENTS

This work was performed while the first author held a National Research Council - NASA Lewis Research Center Research Associateship partially supported by the Army Research Laboratory. The authors are grateful to George W. Leissler and Sandra L. Skotko for their assistance in the preparation of TBC coatings and metallographic specimens, respectively.

APPENDIX A. TOTAL ACCUMULATED CREEP STRAINS IN CERAMIC COATING WITH A CONSTANT ELASTIC MODULUS UNDER STRESS RELAXATION

The creep strain rate for a ceramic coating with a constant Young's modulus that is undergoing stress relaxation can be expressed as

$$\dot{\varepsilon}_p = \frac{d\varepsilon_p}{dt} = A \cdot \exp\left(-\frac{Q}{RT}\right) \cdot \left(\sigma_0 - \varepsilon_p \frac{E_c}{1-\nu_c}\right)^n \cdot t^{-s} \tag{A1}$$

where $\dot{\varepsilon}_p$ and ε_p are the creep strain rate and creep strain, t and T are time and Temperature, A is a constant, n and s are stress and time exponents, respectively, Q is the creep activation energy, is temperature, R is the gas constant, σ_0 is the initial thermal stress in the coating, and E_c and ν_c are the elastic modulus and Poisson's ratio of the ceramic coating. Equation (A1) can be rearranged to give

$$\frac{d\varepsilon_p}{\left(\sigma_0 - \varepsilon_p \frac{E_c}{1-\nu_c}\right)^n} = A \cdot \exp\left(-\frac{Q}{RT}\right) \cdot t^{-s} \cdot dt \tag{A2}$$

Integrating Equation (A2) leads to

$$-\frac{1-\nu_c}{E_c} \frac{\left(\sigma_0 - \varepsilon_p \frac{E_c}{1-\nu_c}\right)^{1-n}}{1-n} \Bigg|_0^{\varepsilon_p} = A \cdot \exp\left(-\frac{Q}{RT}\right) \cdot \frac{t^{1-s}}{1-s} \tag{A3}$$

that is

$$-\frac{1-\nu_c}{E_c(1-n)}\cdot\left[\left(\sigma_0-\varepsilon_p\ \frac{E_c}{1-\nu_c}\right)^{1-n}-\sigma_0^{1-n}\right]=A\cdot\exp\left(-\frac{Q}{RT}\right)\cdot\frac{t^{\,1-s}}{1-s} \tag{A4}$$

Rearrangement of Equation (A3) gives the total accumulated creep strain in the ceramic coating as

$$\varepsilon_p=\left\{\sigma_0-\left[\sigma_0^{1-n}-A\cdot\frac{E_c(1-n)}{(1-\nu_c)(1-s)}\cdot\exp\left(-\frac{Q}{RT}\right)\cdot t^{1-s}\right]^{\frac{1}{1-n}}\right\}\cdot\frac{1-\nu_c}{E_c} \tag{A5}$$

APPENDIX B. THERMAL STRESSES IN THERMAL BARRIER COATING SYSTEMS UNDER STEADY STATE LASER HEATING CONDITIONS

During the steady state laser heating, temperature gradients across the ceramic coating, bond coat and substrate will be established in the thermal barrier coatings. Under the plane stress condition, the corresponding strain components can be obtained by Hooke's law [29]

$$\varepsilon_{ij}=\frac{1+\nu}{E}\sigma_{ij}-\frac{\nu}{E}\delta_{ij}\sigma_{kk}+\delta_{ij}\alpha(T-T_0),\qquad i,j,k=1,2$$

$$\varepsilon_{13}=\varepsilon_{23}=0 \tag{B1}$$

$$\varepsilon_{33}=-\frac{\nu}{E}(\sigma_{11}+\sigma_{22})+\alpha(T-T_0)$$

where is k the dummy suffix and implies summation for all k, δ_{ij} is the Kronecher's delta, ε_{ij} and σ_{ij} are the strain and stress components, E and v are the Young's modulus and Poisson's ratio of the material, and T and T_0 are the steady state heating temperature and initial temperature in the coating. For the coating system in this study, a biaxial stress state can be assumed. Therefore, Equation (B1) can be simplified as

$$\varepsilon_{11}=\varepsilon_{22}=\frac{1-\nu}{E}\sigma+\alpha[T-T_0] \tag{B2a}$$

$$\varepsilon_{33}=-\frac{2\nu}{E}\sigma+\alpha[T-T_0] \tag{B2b}$$

where σ is the in-plane stress in the materials system.

The thermal stresses in the coating systems under the assumed biaxial and no bending conditions can be calculated using force balance and strain compatibility approach. As shown in Figure B1, if a segment of the coating system were constrained in the x-y directions, the in-plane compressive strain and stress will arise upon heating. The constrained thermal strain and stress in the coating system can be generally derived from Equation (B2a) as

$$\varepsilon_{th}(z) = -\alpha(z)\cdot\left[T(z) - T_0\right] \tag{B3a}$$

$$\sigma_{th}(z) = -\frac{E(z)}{1-\nu(z)}\cdot\alpha(z)\cdot\left[T(z) - T_0\right] \tag{B3b}$$

where $\varepsilon_{th}(z)$ and $\sigma_{th}(z)$ are the thermal expansion induced strain and stress under the fully constrained condition at any given depth z, $\alpha(z)$, $E(z)$ and $\nu(z)$ are the thermal expansion coefficient, the Young's modulus and Poisson's ratio of the coating system, respectively. Note from Figure B1, that because of the different materials, and temperature gradients, involved in the coating system, the quantities expressed in Equations (B3a) and (B3b) are functions of depth z. The restrain of the coating system in the x-y directions can be eliminated by applying an equivalent tensile force at the free boundaries. The equivalent boundary force can be calculated as

$$F = -\int_0^{t_{total}} \frac{E(z)}{1-\nu(z)}\cdot\alpha(z)\cdot\left[T(z) - T_0\right]dz \tag{B4}$$

where t_{total} is the total thickness of the coating, $t_{total} = t_c + t_b + t_s$, t_c, t_b and t_s are thicknesses of the ceramic coating, bond coat and substrate, respectively. This equivalent tensile force counterbalances the stresses in Equation (B3b) at the edges of the coating segment, so the mechanical equilibrium, strain compatibility and boundary conditions can be satisfied. The strain and stress resulting from the equivalent boundary force in the coating system can be written as

$$\varepsilon_{eq} = \frac{\int_0^{t_{total}} \alpha(z)\cdot\frac{E(z)}{1-\nu(z)}\cdot\left[T(z) - T_0\right]dz}{\int_0^{t_{total}} \frac{E(z)}{1-\nu(z)}dz} \tag{B5a}$$

$$\sigma_{eq}(z)=\frac{E(z)}{1-\nu(z)}\cdot\frac{\int_0^{t_{total}}\alpha(z)\cdot\frac{E(z)}{1-\nu(z)}\cdot[T(z)-T_0]dz}{\int_0^{t_{total}}\frac{E(z)}{1-\nu(z)}dz} \tag{B5b}$$

Therefore, the thermal stresses induced by the temperature gradients in the coating system can be obtained by the superposition of the stress due to the constrained thermal expansion in Equation (B3b) and the stress due to the equivalent boundary force in Equation (B5b), that is

$$\sigma(z)=-\alpha(z)\cdot\frac{E(z)}{1-\nu(z)}\cdot[T(z)-T_0]+\frac{E(z)}{1-\nu(z)}\cdot\frac{\int_0^{t_{total}}\alpha(z)\cdot\frac{E(z)}{1-\nu(z)}\cdot[T(z)-T_0]dz}{\int_0^{t_{total}}\frac{E(z)}{1-\nu(z)}dz}$$

$$=\frac{E(z)}{1-\nu(z)}\left[\varepsilon_{th}(z)+\varepsilon_{eq}(z)\right] \tag{B6}$$

where $\sigma(z)$ is the thermal stress in the coating system. In particular, for the three layer coating system consisting of ceramic, bond coat and substrate, the stress in each component of the coating system can be written as

$$\sigma_c(z)=\frac{E_c(z)}{1-\nu_c}\left\{-\alpha_c(z)\cdot[T_c(z)-T_0]+\varepsilon_{eq}\right\} \tag{B7a}$$

$$\sigma_b(z)=\frac{E_b(z)}{1-\nu_b}\left\{-\alpha_b(z)\cdot[T_c(z)-T_0]+\varepsilon_{eq}\right\} \tag{B7b}$$

$$\sigma_s(z)=\frac{E_s(z)}{1-\nu_s}\left\{-\alpha_s(z)\cdot[T_s(z)-T_0]+\varepsilon_{eq}\right\} \tag{B7c}$$

and

$$\varepsilon_{eq}=\frac{\int_0^{t_c}\alpha_c(z)\frac{E_c(z)}{1-\nu_c(z)}[T_c(z)-T_0]dz+\int_{t_c}^{t_c+t_b}\alpha_b(z)\frac{E_b(z)}{1-\nu_b(z)}[T_b(z)-T_0]dz+\int_{t_c+t_b}^{t_c+t_b+t_s}\alpha(z)\frac{E_s(z)}{1-\nu_s(z)}[T_s(z)-T_0]dz}{\int_0^{t_c}\frac{E_c(z)}{1-\nu_c(z)}dz+\int_{tc}^{t_c+t_b}\frac{E_b(z)}{1-\nu_b(z)}dz+\int_{t_c+t_b}^{t_c+t_b+t_s}\frac{E_s(z)}{1-\nu_s(z)}dz} \tag{B8}$$

where the subscripts c, b and s refer to the ceramic, bond coat and substrate, respectively. In the calculations, it was assumed that the moduli of the bond coat and substrate were temperature independent and remained constant across the coating thickness, whereas the modulus of the ceramic coating was allowed to change with the coating depth throughout the testing according to the temperature, time and stress dependencies in Equations (6) and (7). The linear thermal expansion coefficients for the ceramic, bond coat and substrate were used for all calculations.

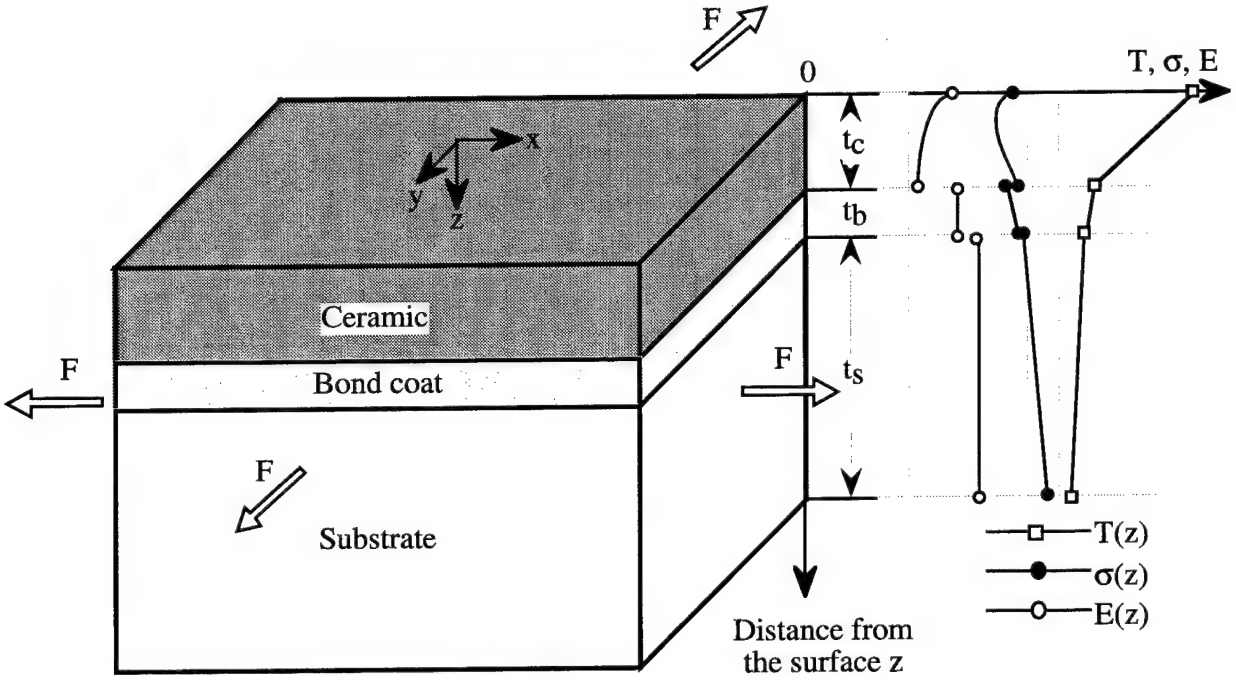

Fig. B1 Schematic diagram showing the principles of the thermal stress calculation in a thermal barrier coating system. The thermal stress gradient, which arises due to the temperature and modulus distributions across the coating, can be determined by the superposition of the stress gradients resulting from the constrained thermal expansion and from the equivalent boundary force F in the system.

APPENDIX C. FINITE DIFFERENCE SINTERING/STRESS RELAXATION MODEL

A finite difference approach was used to solve Equation (2) for the case of time, temperature and/or stress dependent changes in modulus and conductivity. This approach involved repeated calculation of the temperatures, strains, and stresses within the coating and substrate over small increments in time. For the first 3 hours this time increment was 10 seconds (0.00278 hour). The increment was increased to 20 seconds for 3 to 6 hours, then 60 seconds was used up to 11 hours, followed by 600 seconds up to 22 hours and 1200 seconds up to 122 hours. A total of 2179 time steps were employed.

The calculation began at zero time with an elastic stress calculation. The boundary conditions were as follows: the heat flux per unit area passing through the coating and substrate was taken to be $q = 0.48$ MW/m^2 and the initial surface temperature was set to 1368 K consistent with experimental measurements. The ceramic layer was divided into 20 equal sublayers totaling 0.16 cm. Also, four bond coat sublayers totaling 0.0254 cm and 10 substrate sublayers totaling 1.27 cm were employed. Initially each of the ceramic layers was assigned a conductivity of 0.9 W/m-K, the bond coat and substrate conductivity were taken as 11.0 and 46.7 W/m-K, respectively.

The temperature drop across each layer was calculated from

$$q = \frac{k_i}{l_i} \cdot \Delta T_i \tag{C1}$$

where q is the heat flux per unit area, and k_i and l_i are the thermal conductivity and thickness of the i^{th} layer. The average temperature for each layer was taken as the mean of the temperatures of the inner and outer edges of the i^{th} layer. Of course, for the initial elastic case the temperature drop across each sublayer within a given layer are equal.

The elastic (time t=0) analysis continued with a calculation of the thermal strain for each of the 34 layers using thermal expansion coefficients of 10.8×10^{-6} m/m-K for the ceramic, 12.4×10^{-6} m/m-K for the FeCrAlY bond coat and 14.2×10^{-6} m/m-K for the steel substrate. These were calculated using expressions similar to those in Appendix B. Then using assumed initial values of the moduli (27.6 GPa for the ceramic, 137.9 GPa for the bond coat, and 207 GPa for the substrate) the stress in each layer was calculated. The value of ε_{eq}, representing the strain induced by the equivalent boundary forces in the coating system, was calculated from force balance calculation such as described in Appendix B. This term was subtracted from the thermal

strain to give the elastic strain which was further corrected by adding the residual strain generated after coating processing in each component of the coating system. The residual strain and stress in the thermal barrier coating system was calculated using an approach described in an earlier paper [30] . In this particular case, the residual elastic strain added to the ceramic coating was 0.076% which corresponds to the residual stress value of about 28 MPa for the as-sprayed ceramic coating.

Beginning with the second time step, the conductivity and modulus were allowed to vary and the coating stress was allowed to relax according to the expressions discussed in the text. This in turn affected the temperatures, stresses, and strains within the coating. Thermal conductivity was assumed to increase according to published data for sintered plasma sprayed zirconia [19-21] . Sintering data (no external stress) was considered to be appropriate because the stress perpendicular to the interface is expected to be very low. However, the reported data refer to either very porous, yttria fully stabilized zirconia [19-21] or dense yttria partially stabilized zirconia [21] . Thus the available data may be expected to bracket the behavior of the present coating material (yttria partially stabilized zirconia of intermediate porosity). However, as discussed in the text, similar overall results could be obtained with either data set, so the reported results are based solely on the fully stabilized zirconia data.

A new surface temperature was then calculated based on an assumption of constant q and constant backside cooling heat transfer coefficient which implies constant backside substrate temperatures. The temperatures and thermal strains for successive layers were calculated as described above. The moduli were allowed to vary according to Equation (7) in the text using the stress from the prior time step in this calculation. Also, for cases where the stress was decreasing with time, the modulus was held at its highest value. Then the ε_{eq} and the elastic strain were calculated as described above for the first time step. This strain was converted to stress as above except that the stress relaxation term calculated from the previous time step was subtracted from this stress. This approach may begin to reduce the stress beginning with the third time step.

Next, the strain rate was calculated from Equation (2) in the paper, using the terms for s, n and Q given in table 1. The constant A was adjusted until the calculated plastic strain reasonably matched the experimental values. This plastic strain was taken as the strain rate multiplied by the time difference between the present and prior time steps plus the prior accumulated plastic strain. The above steps were repeated 2179 times until the time of 122 hours was reached. The simulated results are illustrated in Figures 12 and 13 in this paper.

REFERENCES

[1] Miller, R. A., "Current Status of Thermal Barrier Coatings - An Overview", *Surface and Coatings Technology*, 30, 1-11, 1987.

[2] Miller, R. A., "Assessment of Fundamental Materials Needs for Thick Thermal Barrier Coatings for Truck Diesel Engines", *NASA Technical Memorandum TM-103130, DOE/NASA/21794-1*, 1990.

[3] Miller, R. A., "Thermal Barrier Coatings for Aircraft Engines - History and Directions", in *Thermal Barrier Coating Workshop, NASA CP-3312* (ed. Brindley, W. J.), 17-34, 1995.

[4] Yonushonis, T. M., "Thick Thermal Barrier Coatings for Diesel Components", *NASA CR-187111*, 1991.

[5] Beardsley, M. B. and Larson, H. J., "Thick Thermal Barrier Coatings for Diesel Components", *DOE/NASA/0332-1, NASA CR - 190759*, 1992.

[6] Kokini, K., Choules, D. B. and Takeuchi, Y., "Thermal Fracture Mechanisms in Ceramic Thermal Barrier Coatings", in *Thermal Barrier Coating Workshop, NASA CP-3312* (ed. Brindley, W. J.), 235-250, 1995.

[7] Kokini, K., Takeuchi, Y. R. and Choules, B. D., "Surface Thermal Cracking of Thermal Barrier Coatings owing to Stress Relaxation: Zirconia vs. Mullite", *Surface and Coatings Technology*, 82, 77-82, 1996.

[8] Zhu, D. and Miller, R. A., "Influence of High Cycle Thermal Loads on Thermal Fatigue Behavior of Thick Thermal Barrier Coatings", *NASA Technical Paper TP-3676, Army Research Laboratory Technical Report ARL-TR-1341*, May 1997.

[9] Zhu, D. and Miller, R. A., "Investigation of Thermal Fatigue Behavior of Thermal Barrier Coatings", in *International Conference on Metallurgical Coatings and Thin Films* 1997. Also *Surface and Coatings Technology*, in press.

[10] Firestone, R. F., Logan, W. R., Adams, J. W. and Bill, R. C. J., "Creep of Plasma-sprayed-ZrO_2 Thermal Barrier Coatings", in *The 6th Annual Conference on Composites and Advanced Ceramic Materials* (eds. Buckley, J. D., Packer, C. M. and Gebhardt, J. J.), 758-771, 1982.

[11] Cruse, T. A., Stewart, S. E. and Ortiz, M., "Thermal Barrier Coating Life Prediction Model Development", in *The Gas Turbine and Aeroengine Congress and Exposition* , 1-8, 88-GT-284, 1988.

[12] DeMasi, J. T., Sheffler, K. D. and Ortiz, M., "Thermal Barrier Coating Life Prediction Model Development: Phase I-Final Report", *NASA CR-182230*, December 1989.

[13] Meier, S. M., Nissely, D. M. and Sheffler, K. D., "Thermal Barrier Coating Life Prediction Model Development: Phase II-Final Report", *NASA CR-182230*, July 1991.

[14] Goedjen, J. G., Brindley, W. J. and Miller, R. A., "Sintering of Plasma-Sprayed Sol Gel Zirconia-Yttria as a Function of Silica Content", in *Advances in Thermal Spray Science and Technology* (eds. Berndt, C. C. and Sampath, S.), 73-77, 1995.

[15] Thurn, G., Schneider, G. A. and Aldinger, F., "High-temperature Deformation of Plasma-sprayed ZrO_2-Thermal Barrier Coatings", *Materials Science and Engineering*, to be published, 1997.

[16] Kingery, W. D., Bowen, H. K. and Uhlmann, D. K., "Introduction to Ceramics", John Wiley & Sons, New York, 1976.

[17] Zhu, D. and Miller, R. A., "Investigation of Thermal Low Cycle and High Cycle Fatigue Mechanisms of Thick Thermal Barrier Coatings", in *The 3rd Thermal Barrier Coating Workshop, sponsored by the TBC Interagency Coordination Committee* (ed. Brindley, W. J.), 139-150, 1997. To be published in *Materials Science and Engineering*.

[18] Wesling, K. F., Socie, D. F. and Beardsley, B., "Fatigue of Thick Thermal Barrier Coatings", *Journal of the American Ceramic Society*, 77, 1863-1868, 1991.

[19] Eaton, H. E., Linsey, J. R. and Dinwiddie, R. B., "The Effect of Thermal Aging on the Thermal Conductivity of Plasma Sprayed Fully Stabilized Zirconia", in *Thermal Conductivity* (eds. Tong, T. W.), 289-300, 22, 1994.

[20] Novak, R. C., "Process, Properties, and Environmental Response of Plasma Sprayed Thermal Barrier Coatings", in *Thermal Barrier Coating Workshop, NASA CP-3312* (ed. Brindley, W. J.), 153-165, 1995.

[21] Dinwiddle, R. B., Beecher, S. C., Porter, W., D. and Nagaraj, A. B., "The Effect of Thermal Aging on the Thermal Conductivity of Plasma Sprayed and EB-PVD Thermal Barrier Coatings", in *The International Gas Turbine and Aeroengine Congress and Exhibition* , 1-7, 96-GT-282, 1996.

[22] Johnsen, B. P., Cruse, T. A., Miller, R. A. and Brindley, W. J., "Compressive Fatigue of a Plasma Sprayed ZrO_2-8%Y_2O_3 and ZrO_2-10%NiCrAlY TTBC", *Journal of Engineering Materials and Technology*, 117, 305-310, 1995.

[23] Okamoto, Y., Ieuji, J., Yamada, Y., Hayashi, K. and Nishikawa, T., "Creep Deformation of Yttria-Stabilized Tetragonal Zirconia (Y-TZP)", in *The Third International Conference on the Science and Technology of Zirconia* (eds. Somiya, S., Yamamoto, N. and Hiroaki, Y.), 565-571, Advances in Ceramics, 24B, 1986.

[24] Jimenez-Melendo, M., Dominguez-Rodriguez, A. and Castaing, J., "Point Defect Concentration Relaxation and Creep Transient in Binary Oxides", *Acta Metall. Mater.*, 43, 3589-3604, 1995.

[25] Schmalzried, H., "Chemical Kinetics of Solids", VCH Verlagsgesellschaft, Weinheim, 1995.

[26] Solmon, H., Chaumont, J., Dolin, C. and Monty, C., "Zr, Y and O Self Diffusion in $Zr_{1-x}Y_xO_{2-x/2}$", in *Ceramic Transactions- Point Defects and Related Properties of Ceramics* (eds. Mason, T. O. and Routbort, J. L.), 175-184, Vol. 24, 1991.

[27] Wakai, F., Murayama, N. and Sakaguchi, S., "Deformation of Superplastic Tetragonal ZrO_2 Polycrystals", in *The Third International Conference on the Science and Technology of Zirconia* (eds. Somiya, S., Yamamoto, N. and Hiroaki, Y.), 583-593, Advances in Ceramics, 24B, 1986.

[28] Martinez-Fernandez, J., Jimenez-Melendo, M. and Dominguez-Rodriguez, A., "High-Temperature Creep of Yttrium-Stabilized Zirconia Single Crystals", *Journal of the American Ceramic Society*, 73, 2452-2456, 1990.

[29] Boley, B. A. and Weiner, J. H., "Theory of Thermal Stresses", John Wiley & Sons, Inc., New York, 1960.

[30] Zhu, D. and Miller, R. A., "Evaluation of Oxidation Damage in Thermal Barrier Coating Systems", in *Fundamental Aspects of High Temperature Corrosion* (eds. Shores, D. A., Rapp, R. A. and Hou, P. Y.), 289-307, PV96-26, 1997. Also *NASA Technical Memorandum TM-107360, Army Research Laboratory Technical Report ARL-TR-1254*, November 1996.

REPORT DOCUMENTATION PAGE

Form Approved
OMB No. 0704-0188

1. AGENCY USE ONLY (*Leave blank*)	2. REPORT DATE	3. REPORT TYPE AND DATES COVERED
	November 1997	Technical Memorandum

4. TITLE AND SUBTITLE

Determination of Creep Behavior of Thermal Barrier Coatings Under Laser Imposed Temperature and Stress Gradients

5. FUNDING NUMBERS

WU–505–23–2U-00
1L161102AH45

6. AUTHOR(S)

Dongming Zhu and Robert A. Miller

7. PERFORMING ORGANIZATION NAME(S) AND ADDRESS(ES)

NASA Lewis Research Center
Cleveland, Ohio 44135–3191
and
U.S. Army Research Laboratory
Cleveland, Ohio 44135–3191

8. PERFORMING ORGANIZATION REPORT NUMBER

E–10930

9. SPONSORING/MONITORING AGENCY NAME(S) AND ADDRESS(ES)

National Aeronautics and Space Administration
Washington, DC 20546–0001
and
U.S. Army Research Laboratory
Adelphi, Maryland 20783–1145

10. SPONSORING/MONITORING AGENCY REPORT NUMBER

NASA TM–113169
ARL–TR–1565

11. SUPPLEMENTARY NOTES

Dongming Zhu, National Research Council—NASA Research Associate at Lewis Research Center, and Robert A. Miller, NASA Lewis Research Center. Responsible person, Robert A. Miller, organization code 5160, (216) 433–3298.

12a. DISTRIBUTION/AVAILABILITY STATEMENT

Unclassified - Unlimited
Subject Categories: 23 and 27 Distribution: Nonstandard

This publication is available from the NASA Center for AeroSpace Information, (301) 621–0390.

12b. DISTRIBUTION CODE

13. ABSTRACT ***(Maximum 200 words)***

In the present study, a laser sintering/creep technique has been established to quantitatively determine the creep behavior of thermal barrier coatings under steady state high heat flux/high thermal gradient conditions. An approach is proposed to separate the strong influence of stress relaxation, based on the deduced strain rate changes with respect to time and temperature during testing. For a plasma sprayed zirconia-8wt.% yttria ceramic coating, a large primary creep strain and a low creep activation energy were observed. The significant primary creep stage and low apparent creep activation energy for the coating are attributed to stress induced mechanical sliding, and temperature and stress enhanced cation diffusion through the splat and grain boundaries. Possible creep mechanisms for the ceramic coating are also discussed. The elastic modulus evolution, the stress response and the total accumulated creep strain variation across the ceramic coating under laser imposed temperature and stress conditions are simulated using a finite difference approach. The modeled creep response is consistent with experimental observations.

14. SUBJECT TERMS

Thermal barrier coating; Laser sintering and creep; Elastic modulus evolution; Stress relaxation

15. NUMBER OF PAGES

47

16. PRICE CODE

A03

17. SECURITY CLASSIFICATION OF REPORT	18. SECURITY CLASSIFICATION OF THIS PAGE	19. SECURITY CLASSIFICATION OF ABSTRACT	20. LIMITATION OF ABSTRACT
Unclassified	Unclassified	Unclassified	